Field Data Analysis and Weather Scenario of a Downburst Event in Livorno, Italy, on 1 October 2012

MASSIMILIANO BURLANDO

Department of Civil, Chemical and Environmental Engineering (DICCA), Polytechnic School, University of Genoa, Genoa, Italy

DJORDJE ROMANIĆ

Wind Engineering, Energy and Environment (WindEEE) Research Institute, Western University, London, Ontario, Canada

GIOVANNI SOLARI

Department of Civil, Chemical and Environmental Engineering (DICCA), Polytechnic School, University of Genoa, Genoa, Italy

HORIA HANGAN

Wind Engineering, Energy and Environment (WindEEE) Research Institute, Western University, London, Ontario, Canada

SHI ZHANG

School of Civil Engineering, and Key Laboratory of Structural Wind Engineering and Urban Wind Environment, Beijing Jiaotong University, Beijing, China

(Manuscript received 24 January 2017, in final form 15 May 2017)

ABSTRACT

The Mediterranean is a ''hot spot'' for the genesis of different types of severe weather events, including potentially damaging wind phenomena like downbursts, whose occurrence and evolution in this geographical region have not been documented in the literature. This paper is part of an interdisciplinary collaboration between atmospheric scientists and wind engineers with the objective of conducting a comprehensive analysis of the field measurements and weather scenarios related to nonsynoptic wind systems in this area. The downburst that struck the Livorno coast of Italy at about 1310 local time 1 October 2012 is investigated as a relevant test case for such severe wind events. The wind velocity records detected by ultrasonic anemometers, part of a monitoring network created for the European ''Wind and Ports'' and ''Wind, Ports and Sea'' projects, are analyzed and decomposed in order to inspect the main statistical features of this transient event. The analysis of the meteorological precursors to this event is carried out making use of model analyses, standard in situ measurements, remote sensing techniques, proxy data, and direct observations. The results obtained bring new insights into a downburst's onset and detection in the Mediterranean, its evolution at the local scale, and possible connections to specific synoptic-scale weather conditions like secondary cyclogenesis in the lee of the Alps.

1. Introduction

The Gulf of Genoa is a well-known cyclogenesis area (Trigo et al. 2002). Moreover, the Mediterranean basin has the highest frequency of occurrence of cyclones around the globe (Petterssen 1956; Radinović 1987). Ground-breaking studies on this subject performed by Petterssen (1956) and Klein (1957) demonstrated that the Mediterranean, and the western Mediterranean in particular, are areas characterized by very high cyclonic activity in winter. In the late 1980s, Radinović (1987) and Genoveś and Jansà (1989) reported that the number of cyclones in the western Mediterranean is even larger than previously documented. Furthermore, Radinović (1987) demonstrated that Mediterranean cyclones are one of the major climate and weather factors in the

Denotes content that is immediately available upon publication as open access.

Corresponding author: Massimiliano Burlando, massimiliano.burlando@unige.it

DOI: 10.1175/MWR-D-17-0018.1

Mediterranean. These findings were later refined using a number of objective methods for cyclone detection and tracking (e.g., Maheras et al. 2001; Flocas et al. 2010; Kouroutzoglou et al. 2011; Romanić et al. 2016a). Although Mediterranean cyclones should not be confused with extratropical cyclones that form in the North Atlantic (Trigo et al. 1999), they are nevertheless associated with a number of severe weather phenomena in the Mediterranean and nearby regions (Lionello et al. 2006). Detailed investigations of extreme weather in the Mediterranean are of particular importance since this region is identified as one of the two most susceptible regions for the predicted climate changes (Giorgi 2006).

Downbursts, although being severe weather phenomena, have not been extensively researched in the Mediterranean when compared to the research oriented toward the local winds in that region (Burlando 2009). These weather phenomena are defined as strong downdrafts originating from thunderstorm (cumulonimbus) or other cumuliform clouds (e.g., altocumulus or cumulus) (Byers and Braham 1949). Damaging surface winds in intense downbursts can be as high as $75\,\mathrm{m\,s^{-1}}$ (Fujita 1990). Yet another classification of downbursts is as wet or dry depending on whether downburst events are accompanied by precipitation or not, respectively. It has been observed that dry downbursts are typically produced in high-based cumulonimbus or altocumulus clouds (Wakimoto 1985), whereas wet downbursts are usually associated with well-developed thunderstorms (Atkins and Wakimoto 1991; Straka and Anderson 1993). Dry downbursts occur when the ambient temperature lapse rate below the cloud base is close to dry adiabatic or even superadiabatic in the surface boundary layer (Wakimoto 1985). While descending below the cloud base, the downdraft temperature first increases following the moist-adiabatic lapse rate until all raindrops evaporate, after which the temperature follows the dry-adiabatic lapse rate. In contrast to this dry microburst sounding model, the subcloud dry-adiabatic layer is shallower and the lower-atmospheric levels are moister when wet downbursts occur (Proctor 1989).

Most downburst-related studies are based on or validated against the meteorological data obtained above the continental parts of the United States [e.g., the abovementioned pioneering studies performed by Byers, Braham, and Fujita, and many others carried out by Goff (1976), Wakimoto (1985), Hjelmfelt (1988), Holmes et al. (2008), Lombardo et al. (2014), and Gunter and Schroeder (2015)], the Asia–Pacific region (Gomes and Vickery 1976; Sherman 1987; Takayama et al. 1997; Choi 1999, 2004; Geerts 2001; Rowcroft 2011), and a few continental parts of Europe (Järvi et al. 2007; Pistotnik et al. 2011), while none has used meteorological data in the Mediterranean as of yet. Therefore, while greatly contributing to our understanding of the downburst phenomena, the results presented in these studies may have limited geographical applicability. Namely, it is known in meteorology that the microphysics of cumuliform clouds sometimes significantly vary from one geographical region to another (You et al. 2016). Since downbursts are closely coupled with the existence of cumuliform clouds, it is important to understand the geographical precursors for these nonsynoptic storm systems through comprehensive research over different areas around the globe. The Mediterranean region, being a ''hot spot'' for different types of severe weather within the contexts of climate change (Giorgi et al. 2001; Giorgi 2006), heavy rains (Jansa et al. 2001), torrential rains (Alpert et al. 2002), windstorms (Nissen et al. 2010), storm surges (Lionello 2005, 59–65), and lightning (Kotroni and Lagouvardos 2016), is therefore of particular importance and the present study aims at bringing presenting insights into downburst meteorological and surface wind aspects related to this region. Here, a hot spot is defined as a region whose climate is particularly responsive to global change (Giorgi 2006) and severe weather.

In parallel with the extensive research carried out in the atmospheric sciences on the physics and weather precursors of downbursts and transient severe wind events, a number of studies have been performed in wind engineering with reference to the wind loading and response of structures to these phenomena (Letchford et al. 2002). Despite this fact, however, the knowledge of their impact on the built environment is quite fragmentary, and a robust and shared framework is still lacking (Solari 2014). This happens because the complexity of downbursts and nonsynoptic events makes it difficult to establish physically realistic and simple engineering models of the time–space variations of their wind velocity fields. Their short duration and small size make a limited number of reliable data available. Thus, wind loading on structures is mainly still evaluated by means of the model introduced over half a century ago by Davenport (1961) with regard to synoptic cyclones.

To shed new light on this crucial issue and to contribute to our knowledge on downbursts and nonsynoptic severe wind events in an area of the Mediterranean region (i.e., the Ligurian and northern Tyrrhenian Sea), systematic research has recently been undertaken thanks to the creation of an extensive, permanent, and high quality wind monitoring network (section 2) realized for two European Union (EU) projects, ''Wind and Ports'' (WP; Solari et al. 2012) and ''Wind, Ports and Sea'' (WPS; Repetto et al. 2017), which took place in the

period between 2009 and 2015. The Wind Engineering and Structural Dynamics (Windyn) research group at the University of Genoa, which realized these two EU projects and their monitoring network, initially implemented a semiautomatic procedure that separates intense wind events (Gomes and Vickery 1978) into three families (De Gaetano et al. 2014): 1) stationary Gaussian records, basically related to synoptic phenomena; 2) transient nonstationary non-Gaussian records, potentially caused by thunderstorm and convective events; and 3) intermediate records, endowed with typical stationary non-Gaussian features. To process a large amount of data, a separation criterion based on a reduced set of synthetic parameters was adopted (Riera and Nanni 1989; Twisdale and Vickery 1992; Choi and Tanurdjaja 2002; Kasperski 2002; Cook et al. 2003; Durañona et al. 2007; Lombardo et al. 2009) instead of conducting meteorological analyses of multiple events. Based on this tool, a set of transient wind records has been gathered and submitted for statistical evaluations, with the aim of defining the main characteristics of thunderstorms relevant to the wind loading of structures (Solari et al. 2015a). These characteristics have formed the base upon which a novel method to determine the dynamic response of structures to thunderstorm downbursts has been formulated (Solari et al. 2015b; Solari 2016).

Despite its inherent merits, this approach clearly suffers two main shortcomings. The first one is the lack of systematic analyses of the meteorological conditions during thunderstorms. This is a result of the different viewpoints in these two disciplines. In wind engineering, which is mainly oriented to evaluating aerodynamic loads on structures, wind data are usually collected and processed in statistical form, focusing on the limited portion of the atmosphere that includes the built environment, and a comprehensive study of the larger-scale weather phenomena is rather unusual. Atmospheric sciences, oriented toward the analysis of the genesis, morphology, and life cycle of thunderstorms, usually concentrate on the larger scales of atmospheric processes, where the wind is just one of the variables and the surface layer is often treated through integral parameters only. As a result, the scales of motion that the two disciplines focus on are quite different.

The second shortcoming concerns the fact that the single-point time evolution of these phenomena measured with high-sampling-rate sensors can be studied in detail, whereas the limited number of anemometric stations does not allow a detailed description of their evolution in space. Both shortcomings point out the relevant gap that still exists between wind engineering and the atmospheric sciences (Solari 2014), as well as the unexplored potential for filling such gap.

Traditionally the spatial structure of downbursts has been physically simulated by creating an impinging jet over the floor of a test chamber (Wood et al. 2001; Chay and Letchford 2002; Letchford and Chay 2002; Mason et al. 2005; Xu and Hangan 2008; Sengupta and Sarkar 2008; McConville et al. 2009) or tentatively by reproducing only the downburst outflow with a wall jet by modifying the axial flow of a wind tunnel (Lin et al. 2007). In any case, these facilities generate small-scale downbursts in which capturing the details of the outflows and especially the turbulence structure is almost impossible (Zhang et al. 2013). The Wind Engineering Energy and Environment (WindEEE) Dome at Western University, in London, Ontario, Canada, is a unique facility designed to physically simulate downbursts (Hangan 2014). It also offers the unique opportunity to clarify the crucial role of scale effects (Xu et al. 2008; McConville et al. 2009) through comparison with results obtained in other laboratories.

Computational fluid dynamics (CFD) simulations have been applied through full-cloud, subcloud, and impinging wall jet models. The full-cloud model (Orf et al. 2012) offers a comprehensive representation of the whole phenomenon, but fails in allowing fine resolution close to the ground. While it is an important tool for atmospheric sciences, it currently cannot provide relevant information to wind engineering. Thus, wind engineering adopts subcloud (Orf and Anderson 1999; Lin et al. 2007; Mason et al. 2010; Vermeire et al. 2011) and impinging jet (Letchford and Chay 2002; Kim and Hangan 2007; Sengupta and Sarkar 2008; Sim et al. 2016) models relaying on the Reynolds averaged Navier–Stokes (RANS) and large eddy simulation (LES) techniques. Finally, numerical weather prediction (NWP) models are used to simulate atmospheric processes on scales much larger than the downburst-specific models (Lorente-Plazas et al. 2016; Romanić et al. 2016b). As the horizontal grid size in NWPs is typically on the order of 2 km or larger, it is common practice to parameterize the whole cumulus convection process inside the domain. In these situations, the downbursts are subgrid processes.

The huge amount of field measurements provided by the WP and WPS projects represents a great opportunity to analyze these events from a multiscale perspective, using these data as the basis for storm reconstruction and interpretation, as well as serving as a database for future calibration of physical and CFD simulations of real downburst events. The present work is part of a collaboration between Windyn (University of Genoa) and WindEEE (Western University) carried out as an interdisciplinary effort between two groups involving atmospheric scientists and wind engineers, with the

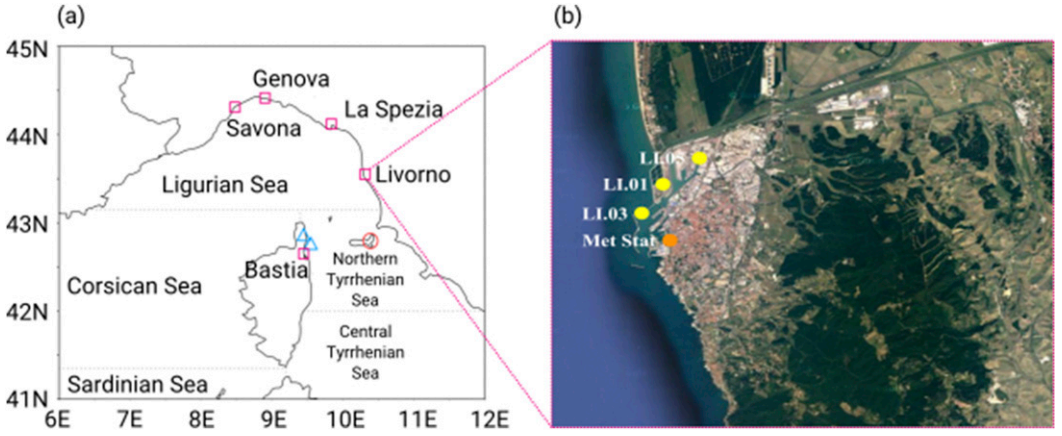

FIG. 1. (a) Map of the northern Mediterranean basin with the international nomenclature of its subbasins, positions where waterspouts occurred on 1 Oct (blue triangles), location of the meteorological radar on Elba (red circle), and positions of cities that are part of the WP measurement network (magenta squares). (b) Map of Livorno with the locations of anemometers LI.01, LI.03, LI05 (yellow circles), and the Laboratorio di Monitoraggio e Modellistica Ambientale (LaMMA) meteorological station (orange circle). See Table 1 for anemometers' coordinates.

objective of conducting a comprehensive analysis of field measurements and weather scenarios related to nonsynoptic wind systems in the Mediterranean. In this paper, the downburst event that struck the Livorno coast of Italy at about 1210 UTC (i.e., 1310 local time) 1 October 2012 is investigated as a test case and a first step toward inspecting the potential of this collaboration. This study uniquely couples synoptic analysis, which describes the atmospheric conditions on large scales prior to and during the downburst event, with the near-surface statistical analyses of the anemometric records, which characterize the transient nature of the downburst on small scales.

2. Field measurements

a. Monitoring network, dataset, and test-case event

WP (2009–12) and WPS (2013–15) were two European projects carried out by Windyn at the University of Genoa (Solari et al. 2012; Repetto et al. 2017) in cooperation with the port authorities of the main commercial ports in the Ligurian Sea and the northern Tyrrhenian Sea, namely Genoa, Savona, La Spezia, Livorno, and Bastia (Fig. 1a). The anemometric monitoring network is made up of 28 ultrasonic anemometers, three weather stations (equipped with an ultrasonic anemometer, barometer, thermometer, and hygrometer), and three lidar wind profilers. This monitoring network constitutes a unique opportunity to detect thunderstorm records, to analyze their results on a statistical basis, and to select specific events of particular interest.

De Gaetano et al. (2014) implemented a semiautomated procedure to extract a selective database of strong wind events that could be considered to a reasonable extent thunderstorm related. Using this procedure, Solari et al. (2015a) identified 64 independent thunderstorms based on nine anemometric datasets between 2011 and 2012. These thunderstorm events were analyzed in order to study their main characteristics relevant to the wind loading of structures. More recently, the analysis has been extended to 14 anemometers between 2011 and 2015, and over 200 transient nonstationary events related to independent thunderstorms or strongly convective events (Zhang et al. 2017). However, so far no single event has been analyzed individually from a meteorological point of view. Here, one of these events, identified by Solari et al. (2015a) in the area of the port of Livorno, has been selected for a comprehensive phenomenological investigation. This event was measured by more than two anemometers, in the only monitored area that is not topographically complex.

The selected event was recorded by three of the five anemometers monitoring the Livorno site (Table 1), as two instruments were out of order at that time. All the instruments are three-axial ultrasonic anemometers with a 10-Hz sampling rate and wind speed and direction precision of 0.01 m s^{-1} and 1°, respectively. Their position was selected in order to register undisturbed wind velocity time histories. The locations of the three anemometers that recorded the event of 1 October (i.e., LI.01, LI.03, and LI.05) are shown in Fig. 1b.

Figure 2 shows the time series of wind speed v and direction α recorded by these anemometers. The order (from top to bottom) of the time series has been chosen to follow the chronological occurrence of this meteorological

TABLE 1. Full composition of the anemometric monitoring network in the port of Livorno during 2012. The positions of the LI.01, LI.03, and LI.05 anemometers are indicated in Fig. 1b.

Code	Geographical coordinates (λ, ϕ) (°N, °E)	Position	Height above ground (m)
LI.01	(43.570, 10.301)	Tower	20
LI.02	(43.583, 10.307)	Tower	20
LI.03	(43.558, 10.290)	Tower	20
LI.04	(43.541, 10.294)	Tower	20
LI.05	(43.580, 10.319)	Building[a]	75

[a] The anemometer is on top of an antenna mast, 2.5 m above the building roof.

event: the anemometer LI.03, which is the closest to the sea, was the first to measure the wind speed increase that occurred at around 1209 UTC, as indicated by the vertical dashed line in Fig. 2a; the anemometers LI.01 and LI.05, which are gradually farther from the coast (see Fig. 1b), measured the same ramp and peak at about 1211 UTC (Fig. 2c) and 1215 UTC (Fig. 2e), respectively. The steady increase in wind speed before the downburst is due to the approach of a gust front that precedes the thunderstorm (Droegemeier and Wilhelmson 1987; Mueller and Carbone 1987). The first maximum value of the peak slightly decreases from the sea toward the land (i.e., from LI.03 to LI.05). The wind direction, which was about from the north until 1150 UTC, backed 90° (i.e., west) at the peak occurrence and then veered to the original direction. The entire event lasted about 20–30 min.

This description resembles a nonstationary event that originated over the sea, and moved inland east or northeastwardly. A spike stronger than the first peak occurred a few minutes after (at LI.03 and LI.05) or concurrent to the peak itself (at LI.01), which may be interpreted as a small-scale jetlike downburst embedded within the larger-scale main downdraft (Fujita 1986; Sherman 1987; Hjelmfelt 1988). Most likely the spike is not caused by a local random fluctuation of wind speed (see also section 2b) since it is observed at all three stations and it is associated with an abrupt clockwise change in wind direction, as clearly illustrated in Figs. 2b and 2f. The wind direction shifts between the first peak and the spike are abrupt (Sherman 1987) and approximately 90° and 130° at LI.03 and LI.05, respectively.

Despite the phenomenon considered here being a single event from the Mediterranean, it is worth comparing the records reported in Fig. 2 to downbursts measured in other parts of the world. The wind records from the United States (Goldman and Sloss 1969; Charba 1974; Wakimoto 1982; Fujita 1981, 1985; Gast and Schroeder 2004; Holmes et al. 2008) and Singapore (Choi 2004) seem to have either a constant background wind speed or a sudden drop in wind speed prior to the downburst. Conversely, the wind records in Figs. 2a and 2c are characterized by a steady increase in wind speed before reaching the downburst ramp up. In these two cases, the wind speed increased by approximately 5 m s^{-1} between 1145 and 1205 UTC and from 1200 to 1210 UTC, respectively. Simultaneously, the wind direction steadily shifted in a counterclockwise direction, reaching approximately 280°–290° before the ramp up at both anemometers (Figs. 2b and 2d).

The reported measurements in Fig. 2 seem to differ from downbursts measured across the continental parts of Europe as well (Järvi et al. 2007; Pistotnik et al. 2011). The downburst recorded in southern Finland (Järvi et al. 2007) was characterized by an intense gust front prior to the downburst, but it lacks the secondary peak in two out of three wind speed records. Surveying the fallen trees around the measuring site, Järvi et al. (2007) concluded that their instruments most likely did not capture the maximum velocities, therefore suggesting the existence of highly localized small-scale downbursts embedded within the parent downburst. Field measurements from Austria (Pistotnik et al. 2011) show two pronounced peaks in both mean and peak wind speeds, but the speed seems to rapidly decrease prior to the downburst. This deceleration of winds prior to the gust front occurs in situations when the front propagates into strong opposing winds (Mahoney 1988). The background winds in the data reported by Pistotnik et al. (2011) were approximately 3 m s^{-1} larger than in the present case.

The anemometer records in Fig. 2, instead, look very similar to the graphs of a weak downburst measured at a suburban area of Brisbane, Australia (Sherman 1987). The wind speed and direction time series at LI.03 (Fig. 2a) are almost identical to the measurements reported by Sherman (1987) at 10 m AGL (Fig. 3). Sherman also measured a temperature decrease of a few degrees Celsius concurrent to the ramp-up time as well as rainfalls during the whole event, both very similar to the measurements presented in section 3b.

Wakimoto (1982) analyzed several data records of weak downbursts measured outside of Chicago, Illinois, using a Doppler radar, radiosondes, and a network of surface measurements. He classified the life cycle of a downburst into four stages (formative, early mature, late mature, and dissipative) and presented measurements for each of these stages. It seems that the reported event resembles downbursts at stages II and III, which are characterized by sudden shifts in wind directions before, during, and after the downbursts, as well as wind speeds between 10 and 30 m s^{-1}. However, his analysis also shows a noticeable decrease in wind speed prior to the arrival of the downburst with the first peak always being

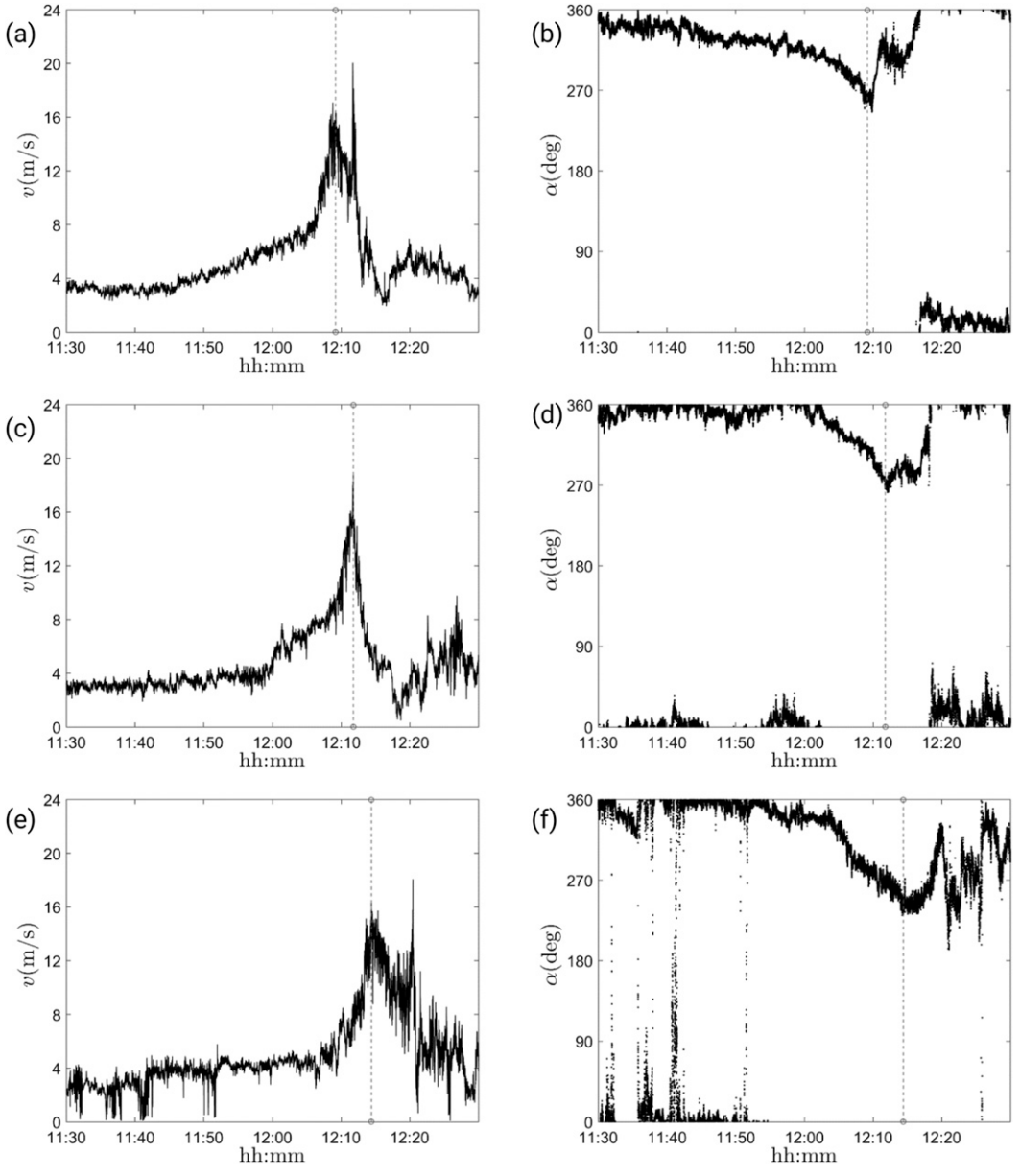

FIG. 2. (left) Wind speed and (right) direction measured by the (a),(b) LI.03; (c).(d) LI.01; and (e),(f) LI.05 anemometers of the port of Livorno monitoring network from 1130 to 1230 UTC 1 Oct 2012. Vertical dashed lines show the approximate times of the gust front passage.

the most pronounced. None of these two features have been observed in the presented case.

The pronounced spike after the first well-defined peak (Figs. 2a,e) has been numerically simulated by Orf et al. (2012). Using a nonhydrostatic LES cloud model (Bryan and Fritsch 2002), they showed a steady increase in wind speed prior to the nonsteady and highly fluctuating downburst peaks, similar to anemometer records in Fig. 2. They reported the existence of a pronounced spike after the first downdraft at a reference point situated along the east flank of the downdraft, whereas the same pattern has not been observed along the west flank of the downdraft.

b. *Signal analysis*

To inspect the characteristics of the wind speed records shown in Fig. 2, the classical decomposition rule of transient wind velocity signals (Choi and Hidayat 2002; Chen and Letchford 2004; Holmes et al. 2008; Kwon and Kareem 2009; Solari et al. 2015a) is herein applied (Figs. 3–5):

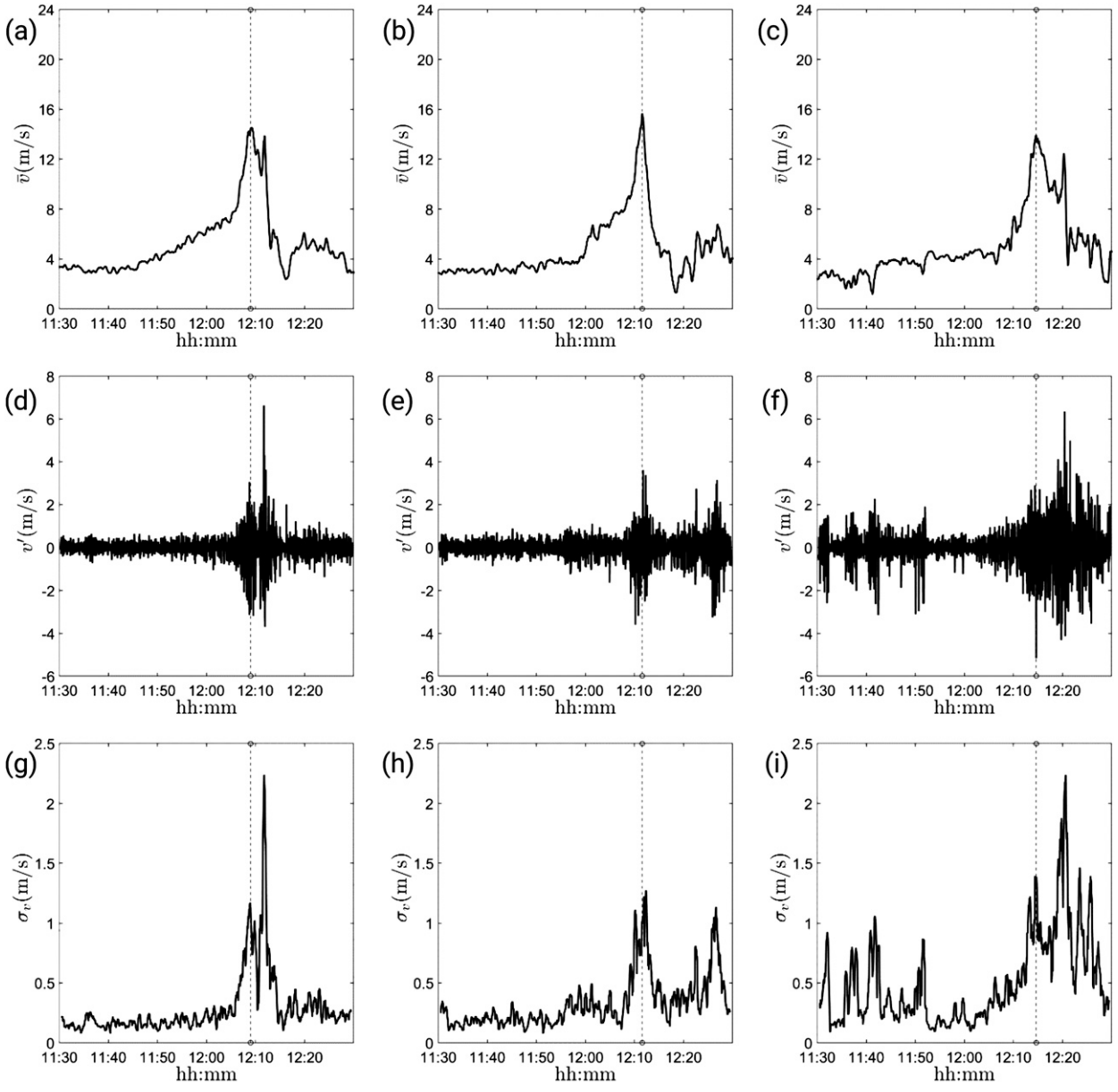

FIG. 3. (top) Slowly varying mean wind velocity, (middle) residual fluctuation, and (bottom) slowly varying standard deviation, as extracted from the records detected by the (a),(d),(g) LI.03; (b),(e),(h) LI.01; and (c),(f),(i) LI.05 anemometers of the port of Livorno monitoring network from 1130 to 1230 UTC 1 Oct 2012. Vertical dashed lines show the approximate times of the gust front passage.

$$v(t) = \bar{v}(t) + v'(t), \tag{1}$$

where $t \in [0, \Delta T]$ is the time; $\Delta T = 1\,\text{h}$ is the period during which the signals are examined; $\bar{v}$ is the slowly varying mean wind velocity, related to the low-frequency content of v; and v' is the residual fluctuation, related to the high-frequency content of v.

The slowly varying mean wind velocity is driven by the large-scale flow. It is often modeled as deterministic and is filtered from the initial signal by a moving average process. The residual fluctuation is induced by the small-scale turbulence and is usually dealt with as a nonstationary random process defined as

$$v'(t) = \sigma_v(t)\tilde{v}'(t), \tag{2}$$

where σ_v is the slowly varying standard deviation of v' and $\tilde{v}'$ is referred to as the reduced turbulent fluctuation. Chen and Letchford (2004) conceptually related the slowly varying standard deviation to the medium scales of motion: on one hand, it is a property of the fluctuation at the turbulence scale; on the other hand, it is driven by

TABLE 2. Synthetic parameters of the wind velocity records. The values related to the secondary peak, if present, are in parentheses.

Parameter	LI.03	LI.01	LI.05
$\hat{v}$ (m s^{-1})	15.81 (18.98)	18.00	15.45 (17.27)
$\overline{v}_{\max}$ (m s^{-1})	14.55 (13.89)	15.66	13.93 (12.46)
G	1.09 (1.37)	1.15	1.11 (1.39)
$\overline{I}_v$(1 h)	0.052	0.074	0.114
$\overline{I}_v$(10 min)	0.070	0.065	0.085
μ'	−0.003	0.000	0.000
σ'	1.003	1.003	1.000
γ'	−0.032	−0.059	−0.125
κ'	2.914	2.863	3.178
L'_v (m)	26.44	28.71	27.08

the mean wind velocity at large scales and it is thus often modeled as deterministic. This interpretation refers to the process of defining and extracting the slowly varying mean. The reduced turbulent fluctuation is then related to the small scales of turbulence and has until now been modeled as a rapidly varying stationary Gaussian random process with zero mean and unit standard deviation (Chen and Letchford 2004; Holmes et al. 2008; Kwon and Kareem 2009; Solari et al. 2015a).

The extraction of $\overline{v}$ from v and of σ_v from v' is herein carried out by a moving average filter (Choi and Hidayat 2002; Holmes et al. 2008) with period $T = 30$ s (Solari et al. 2015a). Other methods are available (McCullough et al. 2014). Replacing Eq. (2) in Eq. (1) gives

$$v(t) = \overline{v}(t)[1 + I_v(t)\tilde{v}'(t)], \tag{3}$$

where

$$I_v(t) = \frac{\sigma_v(t)}{\overline{v}(t)} \tag{4}$$

is the slowly varying turbulence intensity. Since it is usually a weakly dependent function of time, several authors approximate it by its average value over a suitable averaging time period (Chen and Letchford 2004, 2007; Chay et al. 2006; Holmes et al. 2008). Zhang et al. (2017) pointed out that this approximation is questionable since $I_v(t)$ is a non-Gaussian modulating function.

Table 2 shows some synthetic parameters of the wind velocity records. Here, $\hat{v}$, $\overline{v}_{\max}$, and $G = \hat{v}/\overline{v}_{\max}$ are the 1-s peak wind velocity, the maximum value of the slowly varying mean wind velocity, and the gust factor associated with the primary peak, respectively, whereas the values related to the secondary peak, if present, are put in parentheses. For example, $\overline{I}_v$(1 hr) and $\overline{I}_v$(10 min) are the average values of I_v over 1 h and a 10-min interval centered around $\overline{v}_{\max}$ and μ', σ', γ', κ', and L'_v are, respectively, the mean value, standard deviation, skewness, kurtosis, and the integral length scale of the reduced turbulent fluctuation $\tilde{v}'$. The joint analysis of Figs. 3–5 and Table 2 shows that the slowly varying mean wind velocity $\overline{v}$ provides a very clear picture of the movement of the gust front from the sea to the land. It is worth noting that the moving average does not filter out the secondary peak in the LI.03 and LI.05 records, confirming that this peak represents a dominant feature of the large-scale flow. As opposed to the typically adopted wind tunnel modeling approaches, the residual fluctuation v' shows nonstationary random properties with large intensities and intermittency strongly correlated to the largest values of $\overline{v}$. This trend is confirmed by the slowly varying standard deviation σ_v, which exhibits very large values corresponding to the secondary peak detected by the LI.03 and LI.05 anemometers. This observation does not alter the fact that this peak is a dominant feature of the large-scale flow, but points out that its large intensity is significantly enhanced by strong random fluctuations.

The diagrams of the slowly varying turbulence intensity I_v and its average values $\overline{I}_v$ over different time intervals (Fig. 4) confirm that this quantity is not strongly time dependent, except for the presence of some spurious large values that occur when $\overline{v}$ is very small [Eq. (4)], like for instance the spike over 0.3 of LI.01 in correspondence to an almost null $\overline{v}$ value (Fig. 3). In accordance with the results of Solari et al. (2015a) and Zhang et al. (2017), $\overline{I}_v$ ranges between 0.05 and 0.12. Especially on the shorter time scale $\Delta T = 10$ min, $\overline{I}_v$ does not show any significant growth from the sea to the land. This provides a partial confirmation that the time evolution of a downburst is so rapid and short that its wind field does not reach equilibrium conditions over the roughness of the terrain; thus, turbulence intensity is not much affected by this parameter.

The diagrams of the rapidly varying reduced turbulent fluctuation $\tilde{v}'$ in Fig. 5 exhibit the classical random stationary Gaussian features supported by many authors in the literature (Chen and Letchford 2004; Holmes et al. 2008; Solari et al. 2015a). The Gaussian property of the three signals is confirmed by the good agreement between the histogram of $\tilde{v}'$ and the reference Gaussian PDF with $\mu' = 0$ and $\sigma' = 1$; the partial detachment, observed mostly across the middle and right side of the signal, is a consequence of skewness values γ' not exactly equal to 0 and kurtosis values κ' not exactly equal to 3. In addition, the PSD of $\tilde{v}'$ matches the results provided by Solari et al. (2015a). Around $T = 30$ s $S_{\tilde{v}'}$ shows a relative maximum and it decreases with the slope of $n^{-5/3}$ that is typical of the inertial subrange for synoptic-type winds. The integral length scale of the turbulence L'_v has been determined by fitting the experimental PSD by the model proposed by Solari and Piccardo (2001); it is

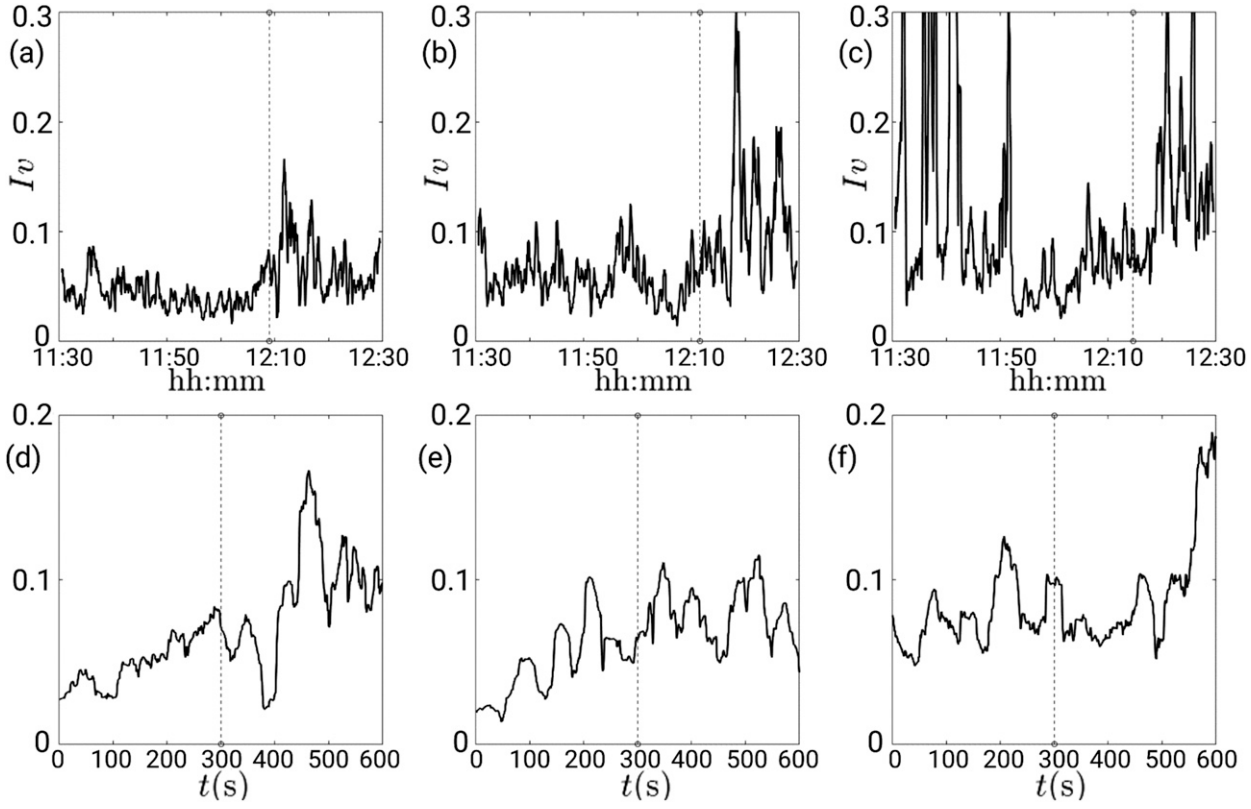

FIG. 4. (top) Slowly varying turbulence intensity I_v over $\Delta T = 1$ h and (bottom) the 10-min interval centered around the time instant at which $\overline{v}_{max}$ occurs, as extracted from the records detected by the (a),(d) LI.03; (b),(e) LI.01; and (c),(f) LI.05 anemometers of the port of Livorno monitoring network from 1130 to 1230 UTC 1 Oct 2012. Vertical dashed lines show the approximate time of the gust front passage.

almost invariant from signal to signal and is fully coherent with the data reported by Solari et al. (2015a). Also, the gust factor G, between 1.11 and 1.39, is coherent with the data reported by Solari et al. (2015a). Slight departures from the universal equilibrium have been previously observed in parts of signals of flows that have sharp interfaces and high intermittency (Braza et al. 2006). This matter deserves further investigation.

This information plays a key role in the evaluation of the behavior of the structures related to downbursts and nonsynoptic severe wind events (Kwon and Kareem 2009; Solari 2016). Unlike synoptic cyclones, where the stationary Gaussian properties of the wind velocity field are rather well known and whose impacts on structures are shared and codified in its essential elements (Davenport 1961), the amount of data available is limited on the duration of the ramp up of the slowly varying mean wind velocity of transient thunderstorm outflows. Moreover, the harmonic content, turbulent fluctuations, and non-Gaussianity, as well as the parameterization of these quantities as functions of time and space, are still not well understood. The collection, interpretation, and modeling of these parameters first for single transient events then for ensembles of homogeneous phenomena are fundamental to filling this gap and opening new prospects aimed at increasing the safety and resiliency of the built environment.

3. Weather scenario and meteorological precursors

a. Synoptic dynamics

The synoptic conditions over Europe on 1 October 2012 are depicted along with the positions of cyclones and anticyclones at 0000 (Fig. 6a) and 1200 UTC (Fig. 6b). The data are obtained from the National Centers for Environmental Prediction's (NCEP) Global Forecast System (GFS) analyses, available on a 0.5° × 0.5° grid. The meteorological situation over Europe was dominated by the presence of Extratropical Cyclone Marianne (following the naming convention used by the Institute of Meteorology of the Freie Universität Berlin, Berlin, Germany) southeast of Iceland, with a surface low pressure minimum below 985 hPa and a trough aloft extending southward to the western Alps. To the east,

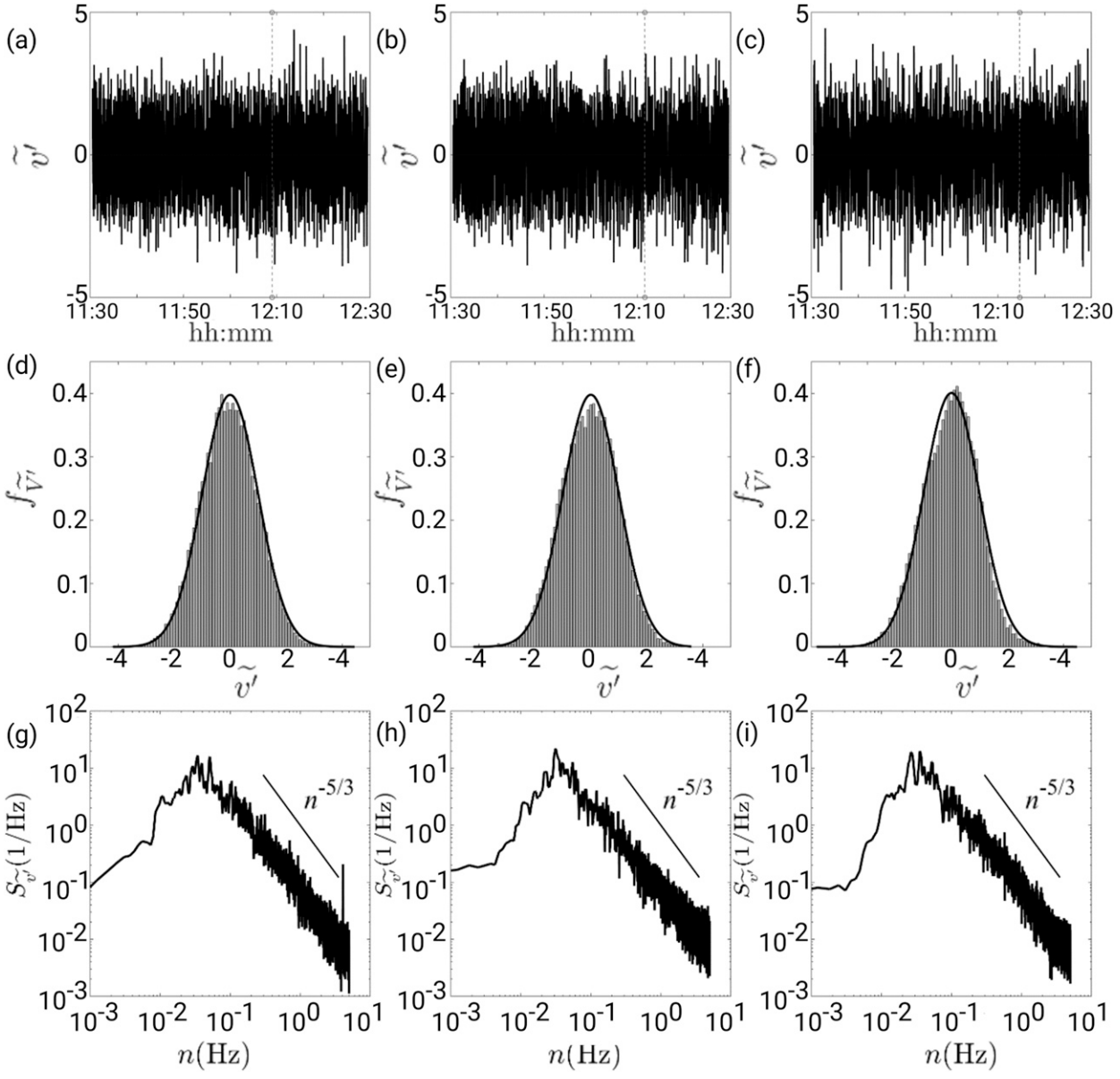

FIG. 5. (top) Rapidly varying reduced turbulence fluctuation, (middle) histogram compared with a reference Gaussian PDF (thick line), and (bottom) PSD, as extracted from the records detected by the (a),(d),(g) LI.03; (b),(e),(h) LI.01; and (c),(f),(i) LI.05 anemometers of the port of Livorno monitoring network from 1130 to 1230 UTC 1 Oct 2012.

the occluded front of Extratropical Cyclone Lulu developed on 25 September in the Labrador Sea and extended from northwestern Russia to north of the Sea of Azov. Finally, the 1025-hPa high pressure maximum associated with Anticyclone Harald, which was situated over central Europe a few days before, had moved over Poland and Ukraine, indicating a blocking situation (Rex 1950).

At 0000 UTC, the tropopause anomaly cut off had a relative minimum of 9870 m and it was located in the northern Mediterranean over the Gulf of Lion (France). The anomaly cutoff moved westward over the Gulf of Genoa at midday. This situation is depicted by the positioning of the 10 000-m height (green contours in Figs. 6a,b). According to GFS analyses, at 1200 UTC the tropopause height showed an abrupt discontinuity along a distance of about 100 km, spanning from less than 10 km over the Gulf of Genoa to more than 13 km over the Corsican Sea (i.e., to the west of Corsica; see Fig. 1a), denoting the existence of a frontal zone beneath.

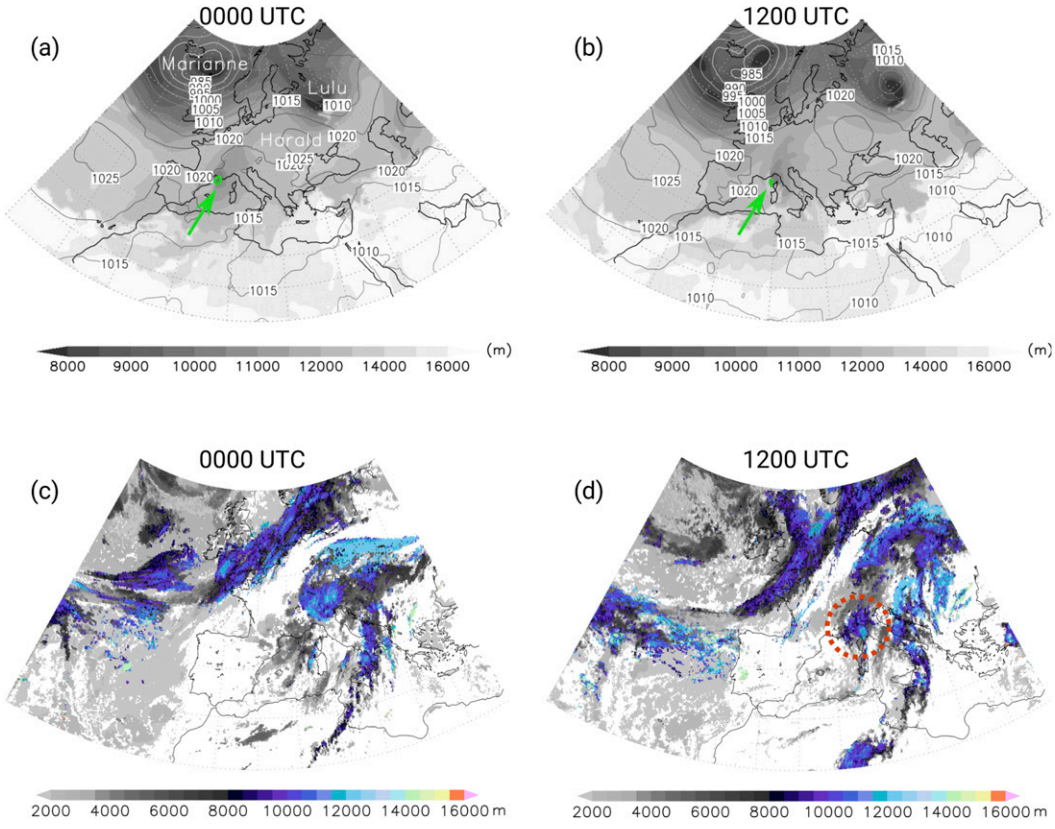

FIG. 6. (a),(b) Mean sea level pressure (contours) and tropopause height (shaded contours) over Europe from GFS analyses. The green contour (indicated with the green arrow) corresponds to the minimum of the tropopause anomaly cutoff over the western Alps. (c),(d) Cloud-top height from Meteosat Second Generation (MSG) data. Results from (left) 0000 and (right) 1200 UTC 1 Oct. The red dashed circle in (d) shows the convective system that developed over the Gulf of Genoa during the morning of 1 Oct.

The distribution of cloud-top heights obtained from the cloud analysis performed by EUMETSAT (EUMETSAT 2013; Derrien et al. 2013) also shows the presence of a smaller cyclone in the eastern Padan plain at 0000 UTC (Fig. 6c). The cyclone, which developed on 29 September as a secondary cyclogenesis event in the Gulf of Genoa (Trigo et al. 2002), had moved over the Balkans at 1200 UTC. However, Fig. 6d shows that a mesoscale convective system, which was only in its embryonic stage at 0000 UTC, developed rapidly over the Gulf of Genoa during the morning. This mesoscale convective system is the main contributor responsible for the strong wind event described in section 2.

Both an upper-level trough upstream of the Alps, like the one of Cyclone Marianne, and a low-level frontal system impinging on the Alps, as denoted by the tropopause discontinuity mentioned above, are considered indispensable meteorological precursors to lee cyclogenesis. These factors play a fundamental role during the rapid trigger phase as a result of the interactions between the frontal zone and mountains (Buzzi and Tibaldi 1978). During this stage, the cyclone deepens while remaining quasi stationary, the upper-level trough fills north of the Alps and deepens to the south, and the jet stream splits northwest of the Alps into a secondary branch over the Mediterranean before reconnecting to the main branch to the north of the Black Sea (Fig. 7). Many different and partially concurrent mechanisms have been proposed for lee cyclogenesis during the trigger phase (Buzzi and Tibaldi 1978; McGinley 1982; Mattocks and Bleck 1986; Bluestein 1995; McTaggart-Cowan et al. 2010a,b). The absolute vorticity fields at the 300-hPa level over Italy at 0000 and 1200 UTC on 1 October are depicted in Figs. 8a and 8b, respectively. Only contours higher than $0.00025\,s^{-1}$ are drawn to indicate the position of the trough (Figs. 6a,b) and its movement from upstream of the Alps to the lee side, where secondary cyclogenesis took place. The conditions favorable for intensification of lee cyclones during their trigger phase (Bluestein 1995; Mattocks and Bleck 1986) were present over the Corsican Sea at 0000 UTC and over the Ligurian Sea at 1200 UTC when the

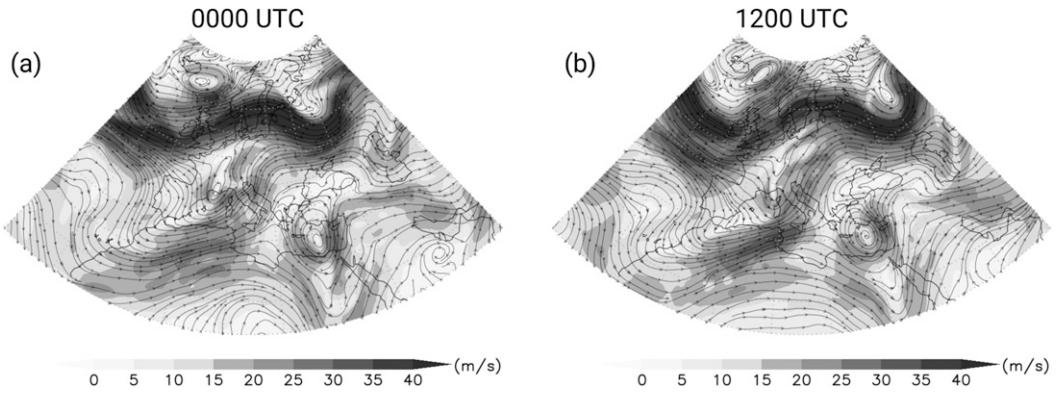

FIG. 7. Wind speed (shaded contours) and streamlines at 300 hPa at (left) 0000 and (right) 1200 UTC 1 Oct.

relative humidity at 700 hPa (Figs. 8a,b) exceeded 99%. At midday, high clouds covered the whole Ligurian Sea and a deep convective system with cloud-top heights above 10 000 m formed and extended from northeast of Corsica to the coast of Tuscany.

Figures 8a and 8b show the mean storm motion (vectors), which is calculated as an integral measure of the wind velocity variation between 0 and 6000 m above sea level (ASL). This parameter is very useful for predicting the spatial evolution of thunderstorms inside complex convective systems. In the present case, the mean storm motion at 1200 UTC in the eastern Ligurian Sea and northern Tyrrhenian Sea (Fig. 8b) was almost purely zonal with an average magnitude of about 6 m s^{-1} to the east. This value is the result of the wind field shift from south-southeast in the lower troposphere (at 925 hPa) to southwest aloft (at 400 hPa). The updrafts turn clockwise as they rise and their corresponding gust fronts occur prevailingly on the eastern side of the convective cells, where new updrafts form (Weisman and Klemp 1982; Fovell and Ogura 1989). The multicell system is driven by the lifting of warm air along the gust front and the system shifts eastward under such wind shear conditions. The storm-relative helicity (SRH), calculated in a layer from 0 to $h = 3000$ m ASL, is another important parameter that helps in determining the type of thunderstorms (Davies-Jones et al. 1990) by measuring the vertical transfer of energy due to the wind shear:

$$\mathrm{SRH} = -\int_0^h \mathbf{k} \cdot (\mathbf{V} - \mathbf{C}) \times \frac{d\mathbf{V}}{dz} dz, \qquad (5)$$

where $\mathbf{V}$ is the environmental wind vector, $\mathbf{C}$ is the storm's translation velocity, and $\mathbf{k} \times d\mathbf{V}/dz$ is the horizontal vorticity with $\mathbf{k}$ being the unit vector in the vertical (z) direction. This index reached its maximum value of 116 $m^2 s^{-2}$ (not shown) 25 km to the west-southwest of Livorno. According to Rasmussen and Blanchard (1998), the calculated values of the mean storm motion and SRH correspond to nonsupercell thunderstorm conditions. It is worth noting, however, that the maximum SRH is above the 75th percentile of the SRH distribution of nonsupercell thunderstorms and very close to the median (124 $m^2 s^{-2}$) of the SRH distribution of supercells without tornadoes. Therefore, the possibility of supercell-like thunderstorms off the coast of Livorno cannot be completely excluded. The SRH, however, should always be interpreted with caution since values above 350 $m^2 s^{-2}$ were observed in intense low-level jets and stable stratification (Romanić et al. 2016b).

b. *Local-scale observations*

According to satellite images (not shown), the deep convective system shown in Fig. 8d started growing to the northeast of Corsica between 0900 and 1000 UTC on 1 October. As reported in the European Severe Weather Database (Dotzek et al. 2009), two waterspouts were observed at 0900 ± 15 min UTC and 1000 ± 15 min UTC at Pietracorbara and Santa Maria di Lota (Corsica), respectively. Their positions are shown in Fig. 1a. Later on, the convective system grew as a multicell complex of thunderstorms positioned along a rather straight line [i.e., a squall line; Zipser (1977)]. Figure 9 shows the reflectivity measured by the meteorological radar installed on the island of Elba, which spans a circular area with radius of about 108 km: Figs. 9a–d show the time evolution of the convective system from 1100 to 1230 UTC with a 30-min time step. At 1100 UTC, the values of radar reflectivity around 30 dBZ show the position of scattered thunderstorms organized along a straight line from Corsica to Tuscany, which slightly shifts to the northeast during the next hour. This observation seems to be coherent with the mean storm motion obtained from the GFS analyses

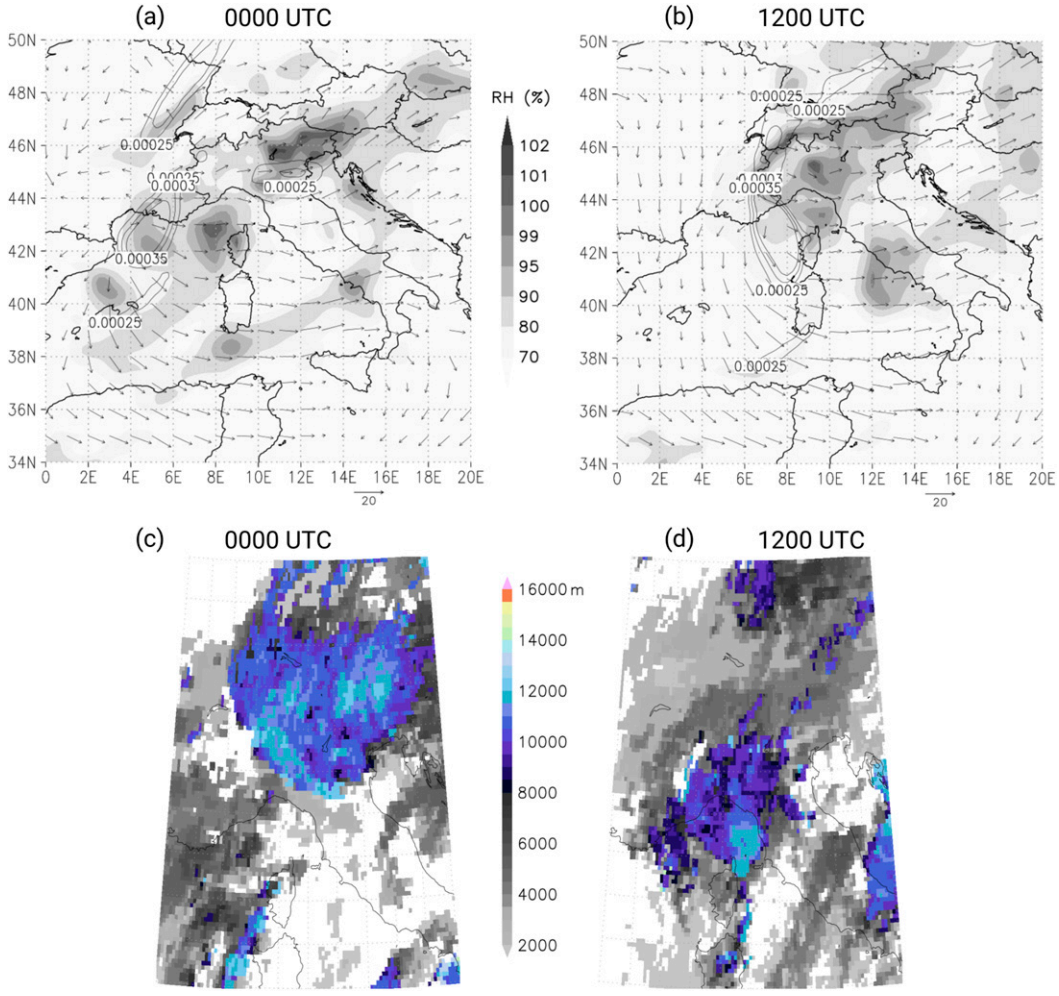

FIG. 8. (a),(b) Relative vorticity (contours) at 300 hPa, relative humidity (shaded contours) at 700 hPa, and mean storm motion (vectors) from GFS analyses. (c),(d) Cloud-top height from MSG data. Results are from (left) 0000 and (right) 1200 UTC 1 Oct.

mentioned in the previous section, as the thunderstorms develop new cells to the right of the mean flow, which is about northward. At 1130 UTC (Fig. 9b), a roughly circular blob appears to the west-southwest of Livorno, in the same position where the maximum SRH value was observed. This convective thunderstorm arrived at 1200 UTC in Livorno (Fig. 9c) and is very likely responsible for the strong wind event depicted in section 2. Unavailability of radar velocity data prevents any firm statement on the existence of a rotating updraft. At 1230 UTC (Fig. 9d), the convective cell had already moved to the north of Livorno. The recorded wind directions during the downburst event (Figs. 2b,d,f), supplemented with the results in Figs. 9c and 9d, suggest that the downburst was spawned in the north part of the convective system. Interestingly, this region is not characterized by the highest radar reflectivity. Takayama et al. (1997) also found that the strongest winds in the mature stage of the downburst were located northwest from the strongest radar reflectivity. The confirmation of this finding is important for downburst forecasting.

The intense convective activity that occurred over the area from Corsica and Tuscany during the morning of 1 October is confirmed by the large number of lightning strikes registered by the Blitzortung network for lightning and thunderstorms (Fig. 10). Lightning strikes were localized in the southern part of the convective system, which is the area populated with the deepest (Figs. 6d and 8d) and most intense convection (Fig. 9c). Lightning strikes were observed in Livorno during this event.

Finally, the weather station located in the city center (Fig. 1b) measured several important parameters during the thunderstorm with a sampling rate of 15 min. The

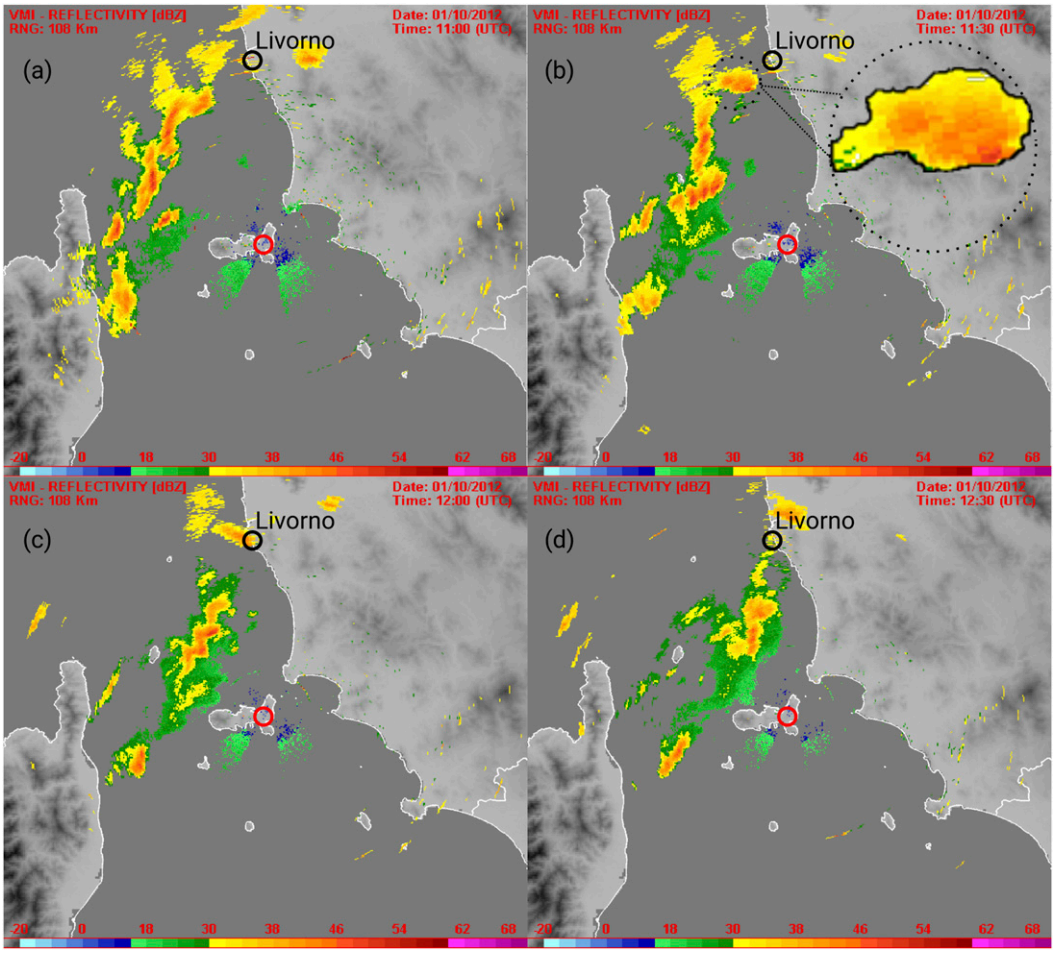

FIG. 9. Reflectivity (dBZ, vertical maximum intensity) measured by the meteorological X-band radar, installed at Cima di Monte (Elba) at 480 m ASL at (a) 1100, (b) 1130, (c) 1200, and (d) 1230 UTC. The location of the meteorological radar on Elba is indicated with a red circle. (Courtesy of the LaMMA Consortium.)

records of wind speed and direction, temperature, solar radiation, and precipitation are reported in Fig. 11. The station measured quite a low mean and maximum wind speed with the prevailing and gust wind directions from the northern sector, as shown in Figs. 11a and 11b. The only wind speed anomaly was registered at 1215 UTC, when both the mean and maximum speeds spiked to 8.5 and 15.8 m s^{-1}, respectively. The temperature also decreased by more than 3° from 21.9°C at 1200 UTC to 18.6°C at 1230 UTC. At the same time, solar radiation dropped from its daily maximum of 1082 W m^{-2} at 1100 UTC to 11.2 W m^{-2} at 1215 UTC, and the rain gauge registered 10.6 mm of precipitation between 1200 and 1215 UTC and 5.6 mm between 1215 and 1230 UTC. The local observations combined with the anemometer records in Fig. 2 confirm that the studied event was a wet downburst (Wakimoto 1982; Atkins and Wakimoto 1991). The pronounced decrease in solar radiation indicates the existence of well-developed and deep thunderstorm clouds in the area.

c. *Instability indices*

In the case of small-scale convective phenomena, many instability indices exist that are intended to provide some deterministic or probabilistic information about the occurrence of severe weather conditions [lifted index (LI), Showalter index, total totals, K index, the severe weather threat index (SWEAT), bulk Richardson number, convective available potential energy (CAPE)]. Three instability indices particularly important for wet downdrafts are the wind index (WINDEX), which can be interpreted as a direct measure of downdraft intensity; LI; and CAPE, which are widely used as measures of updraft intensity. Following the work of Proctor (1989) and

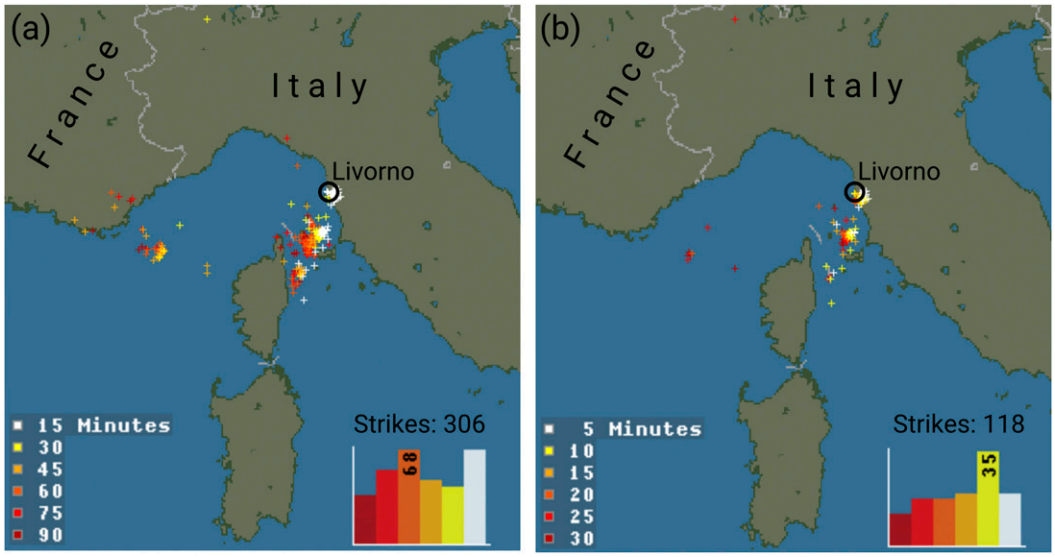

FIG. 10. Strikes recorded (left) from 1100 to 1230 UTC and (right) from 1200 to 1230 UTC 1 Oct by means of the Blitzortung network for lightning and thunderstorms, retrieved through the online archive. (Courtesy of Blitzortung.org.)

Wolfson (1990), McCann (1994) proposed the following expression for WINDEX (WI):

$$\mathrm{WI} = 5\sqrt{H_M R_Q(\Gamma^2 - 30 + Q_L - 2Q_M)}, \qquad (6)$$

where H_M is the height of the melting level above ground (in km), $R_Q = \min(Q_L/12, 1)$, Q_L is the mixing ratio in the first 1 km above the surface, Γ is the temperature lapse rate from the surface to the melting point (in °C km^{-1}), and Q_M is the mixing ratio at the melting level. This parameter tends to replicate the peak wind velocity [in knots (kt, where 1 kt = 0.5144 m s^{-1})].

The WINDEX values calculated at 1200 UTC from GFS data over the Ligurian Sea and northern Tyrrhenian Sea are shown in Fig. 12a. The index is missing where the lapse rate is lower than about 5.5°C km^{-1}, which occurs over the Alps and the eastern Ligurian Apennines. In Livorno, the WINDEX is between 35 and 40, which is similar to the peak velocities (in kt) presented in Fig. 2. The LI and CAPE results at 1200 UTC from GFS data are shown in Figs. 12b and 12c, respectively. Because of the low values of LI (Peppier 1988) and the relatively high values of CAPE, thunderstorms were expected to occur over Corsica, the central Tyrrhenian Sea, the southwestern Alps, and the eastern Padan plain.

The atmospheric soundings from the three stations indicated in Figs. 12a and 12b were also analyzed and the corresponding skew T–log$p$ diagrams are presented in Figs. 12d–f. The WINDEX values evaluated from TEMP messages are 39.5 and 33.5 for LIML (Milan Linate airport) and LIRE (Pratica di Mare Air Force base, Rome), respectively, whereas values were not calculated for LFKJ (airport of Ajaccio, Corsica) as the lapse rate is equal to −5.37°C km^{-1}. The LI results based on radiosoundings are −0.74, −0.70, and −2.07 for LFKJ, LIML, and LIRE, respectively, whereas the CAPE results based on the virtual temperature are 493.4 J kg^{-1} for LFKJ, 315.5 J kg^{-1} for LIML, and 670.9 J kg^{-1} for LIRE.

4. Conclusions and outlook

This paper provides a comprehensive description and interpretation of the field measurements and weather scenario associated with a transient event that struck the Livorno coast of Italy at about 1210 UTC (i.e., 1310 local time) on 1 October 2012. Within the framework of a wide research program dealing with downbursts and nonsynoptic severe wind events, this study pursues a double purpose. First, it provides a survey of a type of meteorological phenomenon widely investigated in many parts of the world but rarely inspected in the Mediterranean. Second, this event has been chosen as a test case with the aim of establishing its real meteorological properties with the potential to improve our understanding, characterization, and modeling of downbursts for wind engineering applications.

The wind speed records detected by three ultrasonic anemometers of the monitoring network created for the European WP and WPS projects have been analyzed and decomposed into component parts to inspect the main features of this event. A statistical analysis for nonstationary wind events has been applied for this case

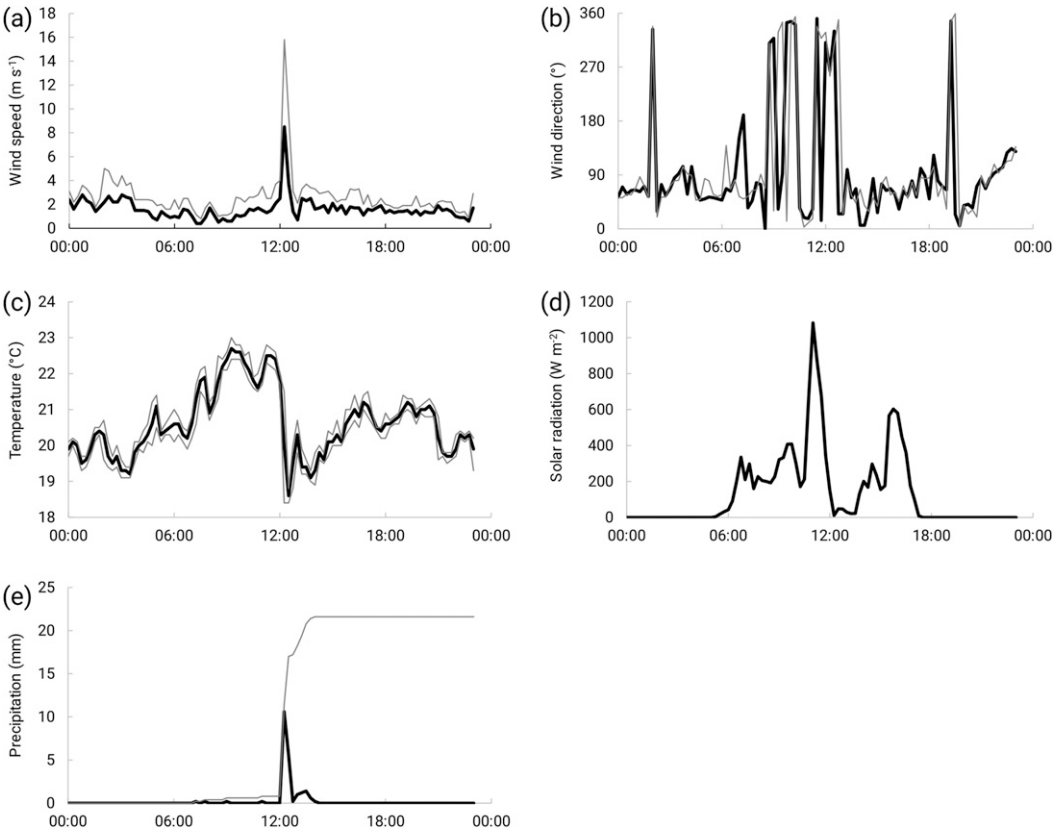

FIG. 11. Measurements from the LaMMA meteorological station in Livorno: (a) mean (black) and maximum (gray) wind speed (m s^{-1}), (b) prevailing (black) and gust (gray) wind directions (°), (c) temperature (black) and its variability (gray) (°C), (d) maximum solar radiation (black) (W m^{-2}), and (e) precipitation (black) and daily cumulated rain (gray) (mm). Data are available every 15 min. (Courtesy of the LaMMA Consortium.)

and the resulting components have been discussed both individually and together. In addition, the joint analysis of different decomposed signals provides some interesting results.

Despite some peculiar aspects of this event, such as the double peak registered by the anemometric sensors, its properties match rather closely with the basic features of the entire database collected by the monitoring network. The set of the slowly varying mean wind velocity components provides a clear picture of the movement of the gust front from the sea to the land. In addition, the results support a robust separation between the dominant features of the large-scale flow and the random turbulent fluctuations. Although the residual fluctuations have strongly nonstationary random properties, the set of diagrams of the slowly varying turbulence intensity confirms that this quantity is not strongly time dependent. The probability density functions of the rapidly varying reduced turbulent fluctuation exhibit classical Gaussian features and its power spectral density tends to decrease in the high-frequency range with a slope that is typical of the inertial subrange of synoptic-type winds.

The analysis of the meteorological conditions concurrent with this event has been carried out by gathering all the meteorological data available in this area and making use of model analyses, standard in situ measurements (surface-observing stations and radio soundings), remote sensing techniques (radar and satellite), proxy data (lightning), and direct observations (from the European Severe Weather Database). All this information contributed to a reconstruction of the weather scenario that occurred on 1 October 2012, over Livorno, confirming that the strong wind event detected by the high-sampling-rate anemometers of the local monitoring network was a wet downburst.

This finding is an important result as it demonstrates the role of specific synoptic-scale conditions over western Europe (e.g., the formation of a secondary cyclone in the lee of the Alps) as an important and common meteorological precursor to the occurrence of local-scale convectively forced severe wind events in the

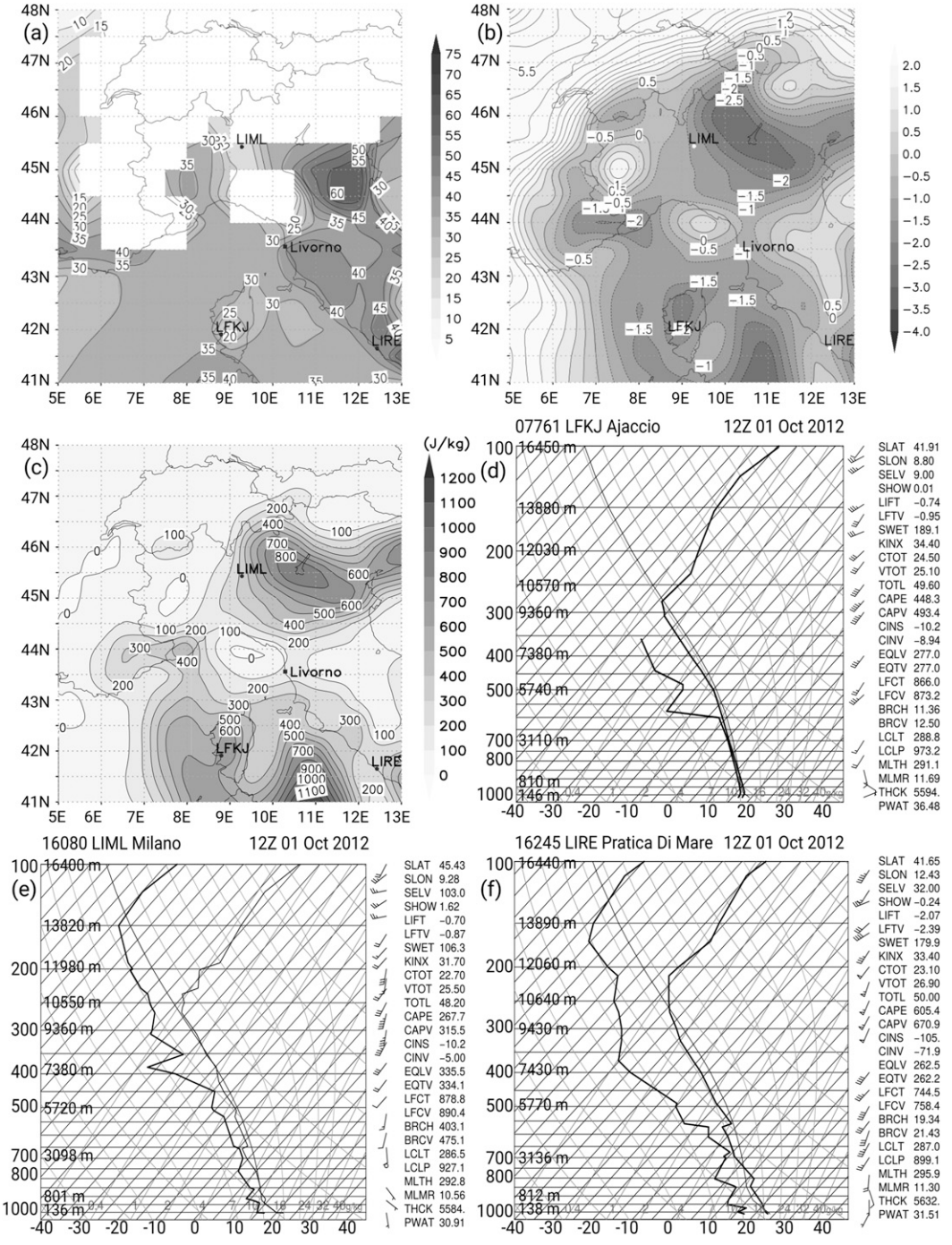

FIG. 12. (a) WINDEX, (b) LI, and (c) CAPE from GFS analyses. Skew T–log$p$ thermodynamic diagrams at (d) Ajaccio, (e) Milan, and (f) Rome. All panels refer to 1200 UTC 1 Oct. (Diagrams courtesy of the University of Wyoming.)

northern Mediterranean. High values of storm-relative helicity and negative values of the lifted index were good indicators of severe weather in the region. The WINDEX values and their location match the downburst observations well.

The high-sampling-rate wind speed records detected within a typical wind engineering framework have proven to be beneficial in analyzing downbursts. Several outcomes from the atmospheric science framework were later refined using the information provided by the

local anemometric network and signal analysis. The present study may therefore form the basis for an extended analysis of nonstationary events in the Mediterranean region using this mixed approach in correlation with the extensive database gathered during the WP and WPS campaigns.

The first implication of this kind of analysis will be its systematic extension to a selection of the most severe wind events recorded by the WP and WPS anemometric network, aiming to distinguish on a statistical basis the events related to convection. The identification of a statistically relevant set of convectively forced severe wind events will represent the starting point for a novel research effort aimed at establishing a robust link between the aforementioned local records and the weather scenarios in which they occur. In turn, this procedure will show to what extent the anemometric records and the meteorological surveys may jointly be used to determine the location of origin, size, and motion pattern of thunderstorms.

The second implication of this research program is strengthening the link between field measurements and analytical, physical, and numerical simulations through the systematic statistical analysis of a broad range of transient events for which high quality measurements are made available. It is fundamental that such evaluations are carried out within the framework of wind tunnel tests and CFD simulations that may establish a closed loop inside which the simulations are used to refine our knowledge of the structure of thunderstorm events detected through local measurements, whereas local measurements are used to calibrate experiments and numerical techniques.

Acknowledgments. The analyses developed at the University of Genoa have been carried out within the framework of the ''Wind monitoring, simulation and forecasting for the smart management and safety of port, urban and territorial systems'' project, financed by Compagnia di San Paolo, with a contribution from the 111 Project via Grant B13002, supported by the Ministry of Education, China, coordinated by Prof. Qingshan Yang of Beijing Jiaotong University, China. Support from the Canada Foundation for Innovation and WindEEE Research Institute at Western University is also acknowledged. Anemometric data have been recorded by the wind monitoring network of the European ''Wind and Ports'' and ''Wind, Ports, and Sea'' projects, funded by the ''Italy France Maritime 2007–2013'' Cross-border Cooperation Programme. The authors thankfully acknowledge the cooperation of the Port Authority of Livorno. Satellite images are based on level 1 data recorded by SEVIRI instrument on board Meteosat Second Generation satellites, operated by EUMETSAT. The LaMMA Consortium (http://www.lamma.rete.toscana.it/) is gratefully acknowledged for radar reflectivity data and measurements from their meteorological station in Livorno. The authors thank the reviewers for their constructive comments that greatly contributed to improving this manuscript.

REFERENCES

Alpert, P., and Coauthors, 2002: The paradoxical increase of Mediterranean extreme daily rainfall in spite of decrease in total values. *Geophys. Res. Lett.*, **29**, doi:10.1029/2001GL013554.

Atkins, N. T., and R. M. Wakimoto, 1991: Wet microburst activity over the southeastern United States: Implications for forecasting. *Wea. Forecasting*, **6**, 470–482, doi:10.1175/1520-0434(1991)006<0470:WMAOTS>2.0.CO;2.

Bluestein, H. B., 1995: *Observations and Theory of Weather Systems*. Vol. II. *Synoptic–Dynamic Meteorology in Midlatitudes*, Oxford University Press, 608 pp.

Braza, M., R. Perrin, and Y. Hoarau, 2006: Turbulence properties in the cylinder wake at high Reynolds numbers. *J. Fluids Struct.*, **22**, 757–771, doi:10.1016/j.jfluidstructs.2006.04.021.

Bryan, G. H., and J. M. Fritsch, 2002: A benchmark simulation for moist nonhydrostatic numerical models. *Mon. Wea. Rev.*, **130**, 2917–2928, doi:10.1175/1520-0493(2002)130<2917:ABSFMN>2.0.CO;2.

Burlando, M., 2009: The synoptic-scale surface wind climate regimes of the Mediterranean Sea according to the cluster analysis of ERA-40 wind fields. *Theor. Appl. Climatol.*, **96**, 69–83, doi:10.1007/s00704-008-0033-5.

Buzzi, A., and S. Tibaldi, 1978: Cyclogenesis in the lee of the Alps: A case study. *Quart. J. Roy. Meteor. Soc.*, **104**, 271–287, doi:10.1002/qj.49710444004.

Byers, H. R., and R. R. Braham, 1949: *The Thunderstorm: Final Report of the Thunderstorm Project*. U.S. Government Printing Office, 287 pp.

Charba, J., 1974: Application of gravity current model to analysis of squall-line gust front. *Mon. Wea. Rev.*, **102**, 140–156, doi:10.1175/1520-0493(1974)102<0140:AOGCMT>2.0.CO;2.

Chay, M. T., and C. W. Letchford, 2002: Pressure distributions on a cube in a simulated thunderstorm downburst. Part A: Stationary downburst observations. *J. Wind Eng. Ind. Aerodyn.*, **90**, 711–732, doi:10.1016/S0167-6105(02)00158-7.

——, F. Albermani, and B. Wilson, 2006: Numerical and analytical simulation of downburst wind loads. *Eng. Struct.*, **28**, 240–254, doi:10.1016/j.engstruct.2005.07.007.

Chen, L., and C. W. Letchford, 2004: A deterministic–stochastic hybrid model of downbursts and its impact on a cantilevered structure. *Eng. Struct.*, **26**, 619–629, doi:10.1016/j.engstruct.2003.12.009.

——, and ——, 2007: Numerical simulation of extreme winds from thunderstorm downbursts. *J. Wind Eng. Ind. Aerodyn.*, **95**, 977–990, doi:10.1016/j.jweia.2007.01.021.

Choi, E. C. C., 1999: Extreme wind characteristics over Singapore—An area in the equatorial belt. *J. Wind Eng. Ind. Aerodyn.*, **83**, 61–69, doi:10.1016/S0167-6105(99)00061-6.

——, 2004: Field measurement and experimental study of wind speed profile during thunderstorms. *J. Wind Eng. Ind. Aerodyn.*, **92**, 275–290, doi:10.1016/j.jweia.2003.12.001.

——, and F. A. Hidayat, 2002: Dynamic response of structures to thunderstorm winds. *Prog. Struct. Eng. Mater.*, **4**, 408–416, doi:10.1002/pse.132.

——, and A. Tanurdjaja, 2002: Extreme wind studies in Singapore. An area with mixed weather system. *J. Wind Eng. Ind. Aerodyn.*, **90**, 1611–1630, doi:10.1016/S0167-6105(02)00274-X.

Cook, N. J., R. I. Harris, and R. Whiting, 2003: Extreme wind speeds in mixed climates revisited. *J. Wind Eng. Ind. Aerodyn.*, **91**, 403–422, doi:10.1016/S0167-6105(02)00397-5.

Davenport, A. G., 1961: The application of statistical concepts to the wind loading of structures. *Proc. Inst. Civ. Eng.*, **19**, 449–472.

Davies-Jones, R., D. W. Burgess, and M. Foster, 1990: Test of helicity as a forecast parameter. Preprints, *16th Conf. on Severe Local Storms*, Kananaskis Park, AB, Canada, Amer. Meteor. Soc., 588–592.

De Gaetano, P., M. P. Repetto, T. Repetto, and G. Solari, 2014: Separation and classification of extreme wind events from anemometric records. *J. Wind Eng. Ind. Aerodyn.*, **126**, 132–143, doi:10.1016/j.jweia.2014.01.006.

Derrien, M., H. Le Gléau, and P. Fernandez, 2013: Algorithm theoretical basis document for ''cloud products.'' Météo-France, Toulouse, France, Rep. SAF/NWC/CDOP/MFL/SCI/ATBD/01, 87 pp. [Available online at http://www.cmsaf.eu/EN/Documentation/Documentation/ATBD/pdf/SAF-NWC-CDOP-MFL-SCI-ATBD-01_v3_2.pdf.]

Dotzek, N., P. Groenemeijer, B. Feuerstein, and A. M. Holzer, 2009: Overview of ESSL's severe convective storms research using the European Severe Weather Database ESWD. *Atmos. Res.*, **93**, 575–586, doi:10.1016/j.atmosres.2008.10.020.

Droegemeier, K. K., and R. B. Wilhelmson, 1987: Numerical simulation of thunderstorm outflow dynamics. Part I: Outflow sensitivity experiments and turbulence dynamics. *J. Atmos. Sci.*, **44**, 1180–1210, doi:10.1175/1520-0469(1987)044<1180:NSOTOD>2.0.CO;2.

Durañona, V., M. Sterling, and C. J. Baker, 2007: An analysis of extreme non-synoptic winds. *J. Wind Eng. Ind. Aerodyn.*, **95**, 1007–1027, doi:10.1016/j.jweia.2007.01.014.

EUMETSAT, 2013: MTG-FCI: ATBD for cloud mask and cloud analysis product. European Organisation for the Exploitation of Meteorological Satellites, Darmstadt, Germany, 60 pp. [Available online at http://www.eumetsat.int/website/wcm/idc/idcplg?IdcService=GET_FILE&dDocName=pdf_atbd_cloud_mask_analysis&RevisionSelectionMethod=LatestReleased&Rendition=Web.]

Flocas, H. A., I. Simmonds, J. Kouroutzoglou, K. Keay, M. Hatzaki, V. Bricolas, and D. Asimakopoulos, 2010: On cyclonic tracks over the eastern Mediterranean. *J. Climate*, **23**, 5243–5257, doi:10.1175/2010JCLI3426.1.

Fovell, R. G., and Y. Ogura, 1989: Effect of vertical wind shear on numerically simulated multicell storm structure. *J. Atmos. Sci.*, **46**, 3144–3176, doi:10.1175/1520-0469(1989)046<3144:EOVWSO>2.0.CO;2.

Fujita, T. T., 1981: Tornadoes and downbursts in the context of generalized planetary scales. *J. Atmos. Sci.*, **38**, 1511–1534, doi:10.1175/1520-0469(1981)038<1511:TADITC>2.0.CO;2.

——, 1985: The downburst: Microburst and macroburst. Satellite and Mesometeorology Research Project, Dept. of the Geophysical Sciences, University of Chicago, Chicago, IL, 136 pp.

——, 1986: DFW microburst on August 2, 1985. 1st ed. Satellite and Mesometeorology Research Project, Dept. of the Geophysical Sciences, University of Chicago, Chicago, IL, 154 pp.

——, 1990: Downburst: Meteorological features and wind field characteristics. *J. Wind Eng. Ind. Aerodyn.*, **36**, 75–86, doi:10.1016/0167-6105(90)90294-M.

Gast, K. D., and S. Schroeder, 2004: Extreme wind events observed in the 2002 Thunderstorm Outflow Experiment. *22nd Conf. on Severe Local Storms*, Hyannis, MA, Amer. Meteor. Soc., 7A.6. [Available online at https://ams.confex.com/ams/11aram22sls/webprogram/Paper81653.html.]

Geerts, B., 2001: Estimating downburst-related maximum surface wind speeds by means of proximity soundings in New South Wales, Australia. *Wea. Forecasting*, **16**, 261–269, doi:10.1175/1520-0434(2001)016<0261:EDRMSW>2.0.CO;2.

Genoveś, A., and A. Jansà, 1989: Statistical approach to mesoscale non-alpine West Mediterranean cyclogenesis. *Report on the Third Session of the Steering Group on Mediterranean Cyclones Study Project*, PSMP Rep. Series 31, WMO TD-298, 77–85.

Giorgi, F., 2006: Climate change hot-spots. *Geophys. Res. Lett.*, **33**, L08707, doi:10.1029/2006GL025734.

——, and Coauthors, 2001: Emerging patterns of simulated regional climatic changes for the 21st century due to anthropogenic forcings. *Geophys. Res. Lett.*, **28**, 3317–3320, doi:10.1029/2001GL013150.

Goff, R. G., 1976: Vertical structure of thunderstorm outflows. *Mon. Wea. Rev.*, **104**, 1429–1440, doi:10.1175/1520-0493(1976)104<1429:VSOTO>2.0.CO;2.

Goldman, J. L., and P. Sloss, 1969: Structure of the leading edge of thunderstorm cold-air outflow. Preprints, *Sixth Conf. on Severe Local Storms*, Chicago, IL, Amer. Meteor. Soc., 75–79.

Gomes, L., and B. J. Vickery, 1976: On thunderstorm wind gusts in Australia. *Civ. Eng. Trans. Ind. Eng. Aust.*, **18**, 33–39.

——, and ——, 1978: Extreme wind speeds in mixed wind climates. *J. Wind Eng. Ind. Aerodyn.*, **2**, 331–344, doi:10.1016/0167-6105(78)90018-1.

Gunter, W. S., and J. L. Schroeder, 2015: High-resolution full-scale measurements of thunderstorm outflow winds. *J. Wind Eng. Ind. Aerodyn.*, **138**, 13–26, doi:10.1016/j.jweia.2014.12.005.

Hangan, H., 2014: The Wind Engineering Energy and Environment (WindEEE) Dome at Western University, Canada. *Wind Eng., Japan Assoc. Wind Eng.*, **39**, 350–351, doi:10.5359/jawe.39.350.

Hjelmfelt, M. R., 1988: Structure and life cycle of microburst outflows observed in Colorado. *J. Appl. Meteor.*, **27**, 900–927, doi:10.1175/1520-0450(1988)027<0900:SALCOM>2.0.CO;2.

Holmes, J. D., H. M. Hangan, J. L. Schroeder, C. W. Letchford, and K. D. Orwig, 2008: A forensic study of the Lubbock-Reese downdraft of 2002. *Wind Struct.*, **11**, 137–152, doi:10.12989/was.2008.11.2.137.

Jansa, A., A. Genoves, M. A. Picornell, J. Campins, R. Riosalido, and O. Carretero, 2001: Western Mediterranean cyclones and heavy rain. Part 2: Statistical approach. *Meteor. Appl.*, **8**, 43–56, doi:10.1017/S1350482701001049.

Järvi, L., and Coauthors, 2007: Micrometeorological observations of a microburst in southern Finland. *Bound.-Layer Meteor.*, **125**, 343–359, doi:10.1007/s10546-007-9204-7.

Kasperski, M., 2002: A new wind zone map of Germany. *J. Wind Eng. Ind. Aerodyn.*, **90**, 1271–1287, doi:10.1016/S0167-6105(02)00257-X.

Kim, J., and H. Hangan, 2007: Numerical simulations of impinging jets with application to downbursts. *J. Wind Eng. Ind. Aerodyn.*, **95**, 279–298, doi:10.1016/j.jweia.2006.07.002.

Klein, W., 1957: Principal tracks and mean frequencies of cyclones and anticyclones in the Northern Hemisphere. U.S. Weather Bureau Paper 40, 60 pp.

Kotroni, V., and K. Lagouvardos, 2016: Lightning in the Mediterranean and its relation with sea-surface temperature. *Environ. Res. Lett.*, **11**, 034006, doi:10.1088/1748-9326/11/3/034006.

Kouroutzoglou, J., H. A. Flocas, K. Keay, I. Simmonds, and M. Hatzaki, 2011: Climatological aspects of explosive cyclones in the Mediterranean. *Int. J. Climatol.*, **31**, 1785–1802, doi:10.1002/joc.2203.

Kwon, D., and A. Kareem, 2009: Gust-front factor: New framework for wind load effects on structures. *J. Struct. Eng.*, **135**, 717–732, doi:10.1061/(ASCE)0733-9445(2009)135:6(717).

Letchford, C. W., and M. T. Chay, 2002: Pressure distributions on a cube in a simulated thunderstorm downburst. Part B: Moving downburst observations. *J. Wind Eng. Ind. Aerodyn.*, **90**, 733–753, doi:10.1016/S0167-6105(02)00163-0.

——, C. Mans, and M. T. Chay, 2002: Thunderstorms—Their importance in wind engineering (a case for the next generation wind tunnel). *J. Wind Eng. Ind. Aerodyn.*, **90**, 1415–1433, doi:10.1016/S0167-6105(02)00262-3.

Lin, W. E., L. G. Orf, E. Savory, and C. Novacco, 2007: Proposed large-scale modelling of the transient features of a downburst outflow. *Wind Struct.*, **10**, 315–346, doi:10.12989/was.2007.10.4.315.

Lionello, P., 2005: *Flooding and Environmental Challenges for Venice and Its Lagoon: State of Knowledge.* Cambridge University Press, 691 pp.

——, and Coauthors, 2006: Chapter 6 cyclones in the Mediterranean region: Climatology and effects on the environment. *Dev. Earth Environ. Sci.*, **4**, 325–372, doi:10.1016/S1571-9197(06)80009-1.

Lombardo, F. T., J. A. Main, and E. Simiu, 2009: Automated extraction and classification of thunderstorm and non-thunderstorm wind data for extreme-value analysis. *J. Wind Eng. Ind. Aerodyn.*, **97**, 120–131, doi:10.1016/j.jweia.2009.03.001.

——, D. A. Smith, J. L. Schroeder, and K. C. Mehta, 2014: Thunderstorm characteristics of importance to wind engineering. *J. Wind Eng. Ind. Aerodyn.*, **125**, 121–132, doi:10.1016/j.jweia.2013.12.004.

Lorente-Plazas, R., P. A. Jiménez, J. Dudhia, and J. P. Montávez, 2016: Evaluating and improving the impact of the atmospheric stability and orography on surface winds in the WRF Model. *Mon. Wea. Rev.*, **144**, 2685–2693, doi:10.1175/MWR-D-15-0449.1.

Maheras, P., H. A. Flocas, I. Patrikas, and C. Anagnostopoulou, 2001: A 40 year objective climatology of surface cyclones in the Mediterranean region: Spatial and temporal distribution. *Int. J. Climatol.*, **21**, 109–130, doi:10.1002/joc.599.

Mahoney, W. P., 1988: Gust front characteristics and the kinematics associated with interacting thunderstorm outflows. *Mon. Wea. Rev.*, **116**, 1474–1492, doi:10.1175/1520-0493(1988)116<1474:GFCATK>2.0.CO;2.

Mason, M., C. W. Letchford, and D. L. James, 2005: Pulsed jet simulation of a stationary thunderstorm downburst. Part A: Physical structure and flow field characterization. *J. Wind Eng. Ind. Aerodyn.*, **93**, 557–580, doi:10.1016/j.jweia.2005.05.006.

——, G. S. Wood, and D. F. Fletcher, 2010: Numerical investigation of the influence of topography on simulated downburst wind fields. *J. Wind Eng. Ind. Aerodyn.*, **98**, 21–33, doi:10.1016/j.jweia.2009.08.011.

Mattocks, C., and R. Bleck, 1986: Jet streak dynamics and geostrophic adjustment processes during the initial stages of lee cyclogenesis. *Mon. Wea. Rev.*, **114**, 2033–2056, doi:10.1175/1520-0493(1986)114<2033:JSDAGA>2.0.CO;2.

McCann, D. W., 1994: WINDEX—A new index for forecasting microburst potential. *Wea. Forecasting*, **9**, 532–541, doi:10.1175/1520-0434(1994)009<0532:WNIFFM>2.0.CO;2.

McConville, A. C., M. Sterling, and C. J. Baker, 2009: The physical simulation of thunderstorm downbursts using an impinging jet. *Wind Struct.*, **12**, 133–149, doi:10.12989/was.2009.12.2.133.

McCullough, M., D. K. Kwon, A. Kareem, and L. Wang, 2014: Efficacy of averaging interval for nonstationary winds. *J. Eng. Mech.*, **140**, 1–19, doi:10.1061/(ASCE)EM.1943-7889.0000641.

McGinley, J., 1982: A diagnosis of Alpine lee cyclogenesis. *Mon. Wea. Rev.*, **110**, 1271–1287, doi:10.1175/1520-0493(1982)110<1271:ADOALC>2.0.CO;2.

McTaggart-Cowan, R., T. J. Galarneau Jr., L. F. Bosart, and J. A. Milbrandt, 2010a: Development and tropical transition of an Alpine lee cyclone. Part I: Case analysis and evaluation of numerical guidance. *Mon. Wea. Rev.*, **138**, 2281–2307, doi:10.1175/2009MWR3147.1.

——, ——, ——, and ——, 2010b: Development and tropical transition of an Alpine lee cyclone. Part II: Orographic influence on the development pathway. *Mon. Wea. Rev.*, **138**, 2308–2326, doi:10.1175/2009MWR3148.1.

Mueller, C. K., and R. E. Carbone, 1987: Dynamics of a thunderstorm outflow. *J. Atmos. Sci.*, **44**, 1879–1898, doi:10.1175/1520-0469(1987)044<1879:DOATO>2.0.CO;2.

Nissen, K. M., G. C. Leckebusch, J. G. Pinto, D. Renggli, S. Ulbrich, and U. Ulbrich, 2010: Cyclones causing wind storms in the Mediterranean: Characteristics, trends and links to large-scale patterns. *Nat. Hazards Earth Syst. Sci.*, **10**, 1379–1391, doi:10.5194/nhess-10-1379-2010.

Orf, L., and J. R. Anderson, 1999: A numerical study of traveling microbursts. *Mon. Wea. Rev.*, **127**, 1244–1258, doi:10.1175/1520-0493(1999)127<1244:ANSOTM>2.0.CO;2.

——, E. Kantor, and E. Savory, 2012: Simulation of a downburst-producing thunderstorm using a very high-resolution three-dimensional cloud model. *J. Wind Eng. Ind. Aerodyn.*, **104–106**, 547–557, doi:10.1016/j.jweia.2012.02.020.

Peppier, R. A., 1988: A review of static instability indices and related thermodynamic parameters. Illinois State Water Survey Miscellaneous Publ. 104, 87 pp. [Available online at http://www.isws.illinois.edu/pubdoc/mp/iswsmp-104.pdf.]

Petterssen, S., 1956: *Motion and Motion Systems*. Vol. I. *Weather Analysis and Forecasting*, 2nd ed. McGraw-Hill, 428 pp.

Pistotnik, G., A. M. Holzer, R. Kaltenböck, and S. Tschannett, 2011: An F3 downburst in Austria—A case study with special focus on the importance of real-time site surveys. *Atmos. Res.*, **100**, 565–579, doi:10.1016/j.atmosres.2010.10.011.

Proctor, F. H., 1989: Numerical simulations of an isolated microburst. Part II: Sensitivity experiments. *J. Atmos. Sci.*, **46**, 2143–2165, doi:10.1175/1520-0469(1989)046<2143:NSOAIM>2.0.CO;2.

Radinović, D., 1987: Mediterranean cyclones and their influence on the weather and climate. Programme on Short- and Medium-Range Weather Prediction Research Rep. 24, WMO, 131 pp.

Rasmussen, E. N., and D. O. Blanchard, 1998: A baseline climatology of sounding-derived supercell and tornado forecast parameters. *Wea. Forecasting*, **13**, 1148–1164, doi:10.1175/1520-0434(1998)013<1148:ABCOSD>2.0.CO;2.

Repetto, M. P., M. Burlando, G. Solari, P. De Gaetano, M. Pizzo, and M. Tizzi, 2017: A web-based GIS platform for the safe management and risk assessment of complex structural and infrastructural systems exposed to wind. *Adv. Eng. Software*, doi:10.1016/j.advengsoft.2017.03.002, in press.

Rex, D. F., 1950: Blocking action in the middle troposphere and its effect upon regional climate. *Tellus*, **2**, 196–211, doi:10.3402/tellusa.v2i3.8546.

Riera, J. D., and L. F. Nanni, 1989: Pilot study of extreme wind velocities in a mixed climate considering wind orientation. *J. Wind Eng. Ind. Aerodyn.*, **32**, 11–20, doi:10.1016/0167-6105(89)90012-3.

Romanić, D., M. Ćurić, M. Lompar, and I. Jovičić, 2016a: Contributing factors to Koshava wind characteristics. *Int. J. Climatol.*, **36**, 956–973, doi:10.1002/joc.4397.

——, ——, M. Zarić, M. Lompar, and I. Jovičić, 2016b: Investigation of an extreme koshava wind episode of 30 January–4 February 2014. *Atmos. Sci. Lett.*, **17**, 199–206, doi:10.1002/asl.643.

Rowcroft, J., 2011: Vertical wind shear profiles in downburst events and the insufficiency of wind turbine design codes. *14th Australasian Wind Engineering Society Workshop*, Canberra, ACT, Australia, AWES, 50–53. [Available online at https://www.awes.org/archives/workshop-proceedings/awes-14/.]

Sengupta, A., and P. P. Sarkar, 2008: Experimental measurement and numerical simulation of an impinging jet with application to thunderstorm microburst winds. *J. Wind Eng. Ind. Aerodyn.*, **96**, 345–365, doi:10.1016/j.jweia.2007.09.001.

Sherman, D. J., 1987: The passage of a weak thunderstorm downburst over an instrumented tower. *Mon. Wea. Rev.*, **115**, 1193–1205, doi:10.1175/1520-0493(1987)115<1193:TPOAWT>2.0.CO;2.

Sim, T. S., M. C. Ong, W. Y. Quek, Z. W. Sum, W. X. Lai, and M. Skote, 2016: A numerical study of microburst-like wind load acting on different block array configurations using an impinging jet model. *J. Fluids Struct.*, **61**, 184–204, doi:10.1016/j.jfluidstructs.2015.11.002.

Solari, G., 2014: Emerging issues and new frameworks for wind loading on structures in mixed climates. *Wind Struct.*, **19**, 295–320, doi:10.12989/was.2014.19.3.295.

——, 2016: Thunderstorm response spectrum technique: Theory and applications. *Eng. Struct.*, **108**, 28–46, doi:10.1016/j.engstruct.2015.11.012.

——, and G. Piccardo, 2001: Probabilistic 3-D turbulence modeling for gust buffeting of structures. *Probab. Eng. Mech.*, **16**, 73–86, doi:10.1016/S0266-8920(00)00010-2.

——, M. P. Repetto, M. Burlando, P. De Gaetano, M. Pizzo, M. Tizzi, and M. Parodi, 2012: The wind forecast for safety management of port areas. *J. Wind Eng. Ind. Aerodyn.*, **104–106**, 266–277, doi:10.1016/j.jweia.2012.03.029.

——, M. Burlando, P. De Gaetano, and M. P. Repetto, 2015a: Characteristics of thunderstorms relevant to the wind loading of structures. *Wind Struct.*, **20**, 763–791, doi:10.12989/was.2015.20.6.763.

——, P. De Gaetano, and M. P. Repetto, 2015b: Thunderstorm response spectrum: Fundamentals and case study. *J. Wind Eng. Ind. Aerodyn.*, **143**, 62–77, doi:10.1016/j.jweia.2015.04.009.

Straka, J. M., and J. R. Anderson, 1993: Numerical simulations of microburst-producing storms: Some results from storms observed during COHMEX. *J. Atmos. Sci.*, **50**, 1329–1348, doi:10.1175/1520-0469(1993)050<1329:NSOMPS>2.0.CO;2.

Takayama, H., H. Niino, S. Watanabe, and J. Sugaya, 1997: Downbursts in the northwestern part of Saitama Prefecture on 8 September 1994. *J. Meteor. Soc. Japan*, **75**, 885–905, doi:10.2151/jmsj1965.75.4_885.

Trigo, I. F., T. D. Davies, and G. R. Bigg, 1999: Objective climatology of cyclones in the Mediterranean region. *J. Climate*, **12**, 1685–1696, doi:10.1175/1520-0442(1999)012<1685:OCOCIT>2.0.CO;2.

——, G. R. Bigg, and T. D. Davies, 2002: Climatology of cyclogenesis mechanisms in the Mediterranean. *Mon. Wea. Rev.*, **130**, 549–569, doi:10.1175/1520-0493(2002)130<0549:COCMIT>2.0.CO;2.

Twisdale, L. A., and P. J. Vickery, 1992: Research on thunderstorm wind design parameters. *J. Wind Eng. Ind. Aerodyn.*, **41**, 545–556, doi:10.1016/0167-6105(92)90461-I.

Vermeire, B. C., L. G. Orf, and E. Savory, 2011: Improved modeling of downburst outflows for wind engineering applications using a cooling source approach. *J. Wind Eng. Ind. Aerodyn.*, **99**, 801–814, doi:10.1016/j.jweia.2011.03.003.

Wakimoto, R. M., 1982: The life cycle of thunderstorm gust fronts as viewed with Doppler radar and rawinsonde data. *Mon. Wea. Rev.*, **110**, 1060–1082, doi:10.1175/1520-0493(1982)110<1060:TLCOTG>2.0.CO;2.

——, 1985: Forecasting dry microburst activity over the high plains. *Mon. Wea. Rev.*, **113**, 1131–1143, doi:10.1175/1520-0493(1985)113<1131:FDMAOT>2.0.CO;2.

Weisman, M. L., and J. B. Klemp, 1982: The dependence of numerically simulated convective storms on vertical wind shear and buoyancy. *Mon. Wea. Rev.*, **110**, 504–520, doi:10.1175/1520-0493(1982)110<0504:TDONSC>2.0.CO;2.

Wolfson, M. M., 1990: Understanding and predicting microbursts. Ph.D. thesis, Massachusetts Institute of Technology, 303 pp. [Available online at http://dspace.mit.edu/handle/1721.1/13970.]

Wood, G. S., K. C. S. Kwok, N. A. Motteram, and D. F. Fletcher, 2001: Physical and numerical modelling of thunderstorm downburst. *J. Wind Eng. Ind. Aerodyn.*, **89**, 535–552, doi:10.1016/S0167-6105(00)00090-8.

Xu, Z., and H. Hangan, 2008: Scale, boundary and inlet condition effects on impinging jets with application to downburst simulations. *J. Wind Eng. Ind. Aerodyn.*, **96**, 2383–2402, doi:10.1016/j.jweia.2008.04.002.

——, ——, and P. Yu, 2008: Analytical solutions for a family of Gaussian impinging jets. *ASME J. Appl. Mech.*, **75**, 021019, doi:10.1115/1.2775502.

You, C.-H., D.-I. Lee, M.-Y. Kang, and H.-J. Kim, 2016: Classification of rain types using drop size distributions and polarimetric radar: Case study of a 2014 flooding event in Korea. *Atmos. Res.*, **181**, 211–219, doi:10.1016/j.atmosres.2016.06.024.

Zhang, S., G. Solari, P. De Gaetano, M. Burlando, and M. P. Repetto, 2017: A refined analysis of thunderstorm outflow characteristics relevant to the wind loading of structures. *Probab. Eng. Mech.*, doi:10.1016/j.probengmech.2017.06.003, in press.

Zhang, Y., H. Hu, and P. P. Sarkar, 2013: Modeling of microburst outflows using impinging jet and cooling source approaches and their comparison. *Eng. Struct.*, **56**, 779–793, doi:10.1016/j.engstruct.2013.06.003.

Zipser, E. J., 1977: Mesoscale and convective-scale downdrafts as distinct components of squall-line structure. *Mon. Wea. Rev.*, **105**, 1568–1589, doi:10.1175/1520-0493(1977)105<1568:MACDAD>2.0.CO;2.